



HAL
open science

Spatial and temporal variability of zooplankton off New Caledonia (Southwestern Pacific) from acoustics and net measurements

Houssem Smeti, Marc Pagano, Christophe E. Menkès, Anne Lebourges-Dhaussy, Brian P. V. Hunt, Valérie Allain, Martine Rodier, Florian de Boissieu, Élodie Kestenare, Cherif Sammari

► To cite this version:

Houssem Smeti, Marc Pagano, Christophe E. Menkès, Anne Lebourges-Dhaussy, Brian P. V. Hunt, et al.. Spatial and temporal variability of zooplankton off New Caledonia (Southwestern Pacific) from acoustics and net measurements. *Journal of Geophysical Research. Oceans*, 2015, 120 (4), pp.2676-2700. 10.1002/2014JC010441 . hal-01162985

HAL Id: hal-01162985

<https://hal.sorbonne-universite.fr/hal-01162985v1>

Submitted on 29 Jun 2017

HAL is a multi-disciplinary open access archive for the deposit and dissemination of scientific research documents, whether they are published or not. The documents may come from teaching and research institutions in France or abroad, or from public or private research centers.

L'archive ouverte pluridisciplinaire **HAL**, est destinée au dépôt et à la diffusion de documents scientifiques de niveau recherche, publiés ou non, émanant des établissements d'enseignement et de recherche français ou étrangers, des laboratoires publics ou privés.

RESEARCH ARTICLE

10.1002/2014JC010441

Key Points:

- Acoustic measurements of zooplankton from an ADCP, an echosounder and a TAPS
- Zooplankton migration and composition are linked to water mass temperatures
- Mesoscale eddies and fronts can substantially enhance zooplankton biomass

Correspondence to:

H. Smeti,
houssem.smeti@gmail.com

Citation:

Smeti, H., M. Pagano, C. Menkes, F. Boissieu, A. Lebourges-Dhaussy, B. P. V. Hunt, V. Allain, M. Rodier, E. Kestenare, and C. Sammari (2015), Spatial and temporal variability of zooplankton off New Caledonia (Southwestern Pacific) from acoustics and net measurements, *J. Geophys. Res. Oceans*, 120, 2676–2700, doi:10.1002/2014JC010441.

Received 10 SEP 2014

Accepted 25 FEB 2015

Accepted article online 13 MAR 2015

Published online 11 APR 2015

Spatial and temporal variability of zooplankton off New Caledonia (Southwestern Pacific) from acoustics and net measurements

Houssem Smeti^{1,2,3}, Marc Pagano¹, Christophe Menkes², Anne Lebourges-Dhaussy⁴, Brian P. V. Hunt^{1,5}, Valerie Allain⁶, Martine Rodier⁷, Florian de Boissieu², Elodie Kestenare⁸, and Cherif Sammari³

¹Mediterranean Institute of Oceanography, Marseille, France, ²LOCEAN Laboratory, Institut de Recherche pour le Développement, Nouméa, New Caledonia, ³National Institute of Marine Sciences and Technologies, Salammbô, Tunisia, ⁴Institut de Recherche pour le Développement, LEMAR laboratory, Bretagne, Plouzané, France, ⁵Department of Earth Ocean and Atmospheric Sciences, University of British Columbia, Vancouver, Canada, ⁶Secretariat of the Pacific Community, Nouméa, New Caledonia, ⁷Institut de Recherche pour le Développement, Papeete, Tahiti, French Polynesia, ⁸Institut de Recherche pour le Développement, LEGOS Laboratory, Toulouse, France

Abstract Spatial and temporal distribution of zooplankton off New Caledonia in the eastern Coral Sea was studied during two multidisciplinary cruises in 2011, during the cool and the hot seasons. Acoustic measurements of zooplankton were made using a shipborne acoustic Doppler current profiler (S-ADCP), a scientific echosounder and a Tracor acoustic profiling system (TAPS). Relative backscatter from ADCP was converted to biomass estimates using zooplankton weights from net-samples collected during the cruises. Zooplankton biomass was estimated using four methods: weighing, digital imaging (ZooScan), ADCP and TAPS. Significant correlations were found between the different biomass estimators and between the backscatters of the ADCP and the echosounder. There was a consistent diel pattern in ADCP derived biomass and echosounder backscatter resulting from the diel vertical migration (DVM) of zooplankton. Higher DVM amplitudes were associated with higher abundance of small zooplankton and cold waters to the south of the study area, while lower DVM amplitudes in the north were associated with warmer waters and higher abundance of large organisms. Zooplankton was largely dominated by copepods (71–73%) among which calanoids prevailed (40–42%), with *Paracalanus* spp. as the dominant species (16–17%). Overall, zooplankton exhibited low abundance and biomass (mean night dry biomass of 4.7 ± 2.2 mg m³ during the cool season and 2.4 ± 0.4 mg m³ during the hot season) but high richness and diversity (Shannon index ~ 4). Substantially enhanced biomass and abundance appeared to be episodically associated with mesoscale features contributing to shape a rather patchy zooplankton distribution.

1. Introduction

Zooplankton hold a key role in the pelagic ecosystem of the World Ocean as a pivotal component of the food web facilitating the transfer of the organic matter produced by the primary levels to higher trophic levels (e.g., micronekton and fish). This energy transfer from primary producers to top predators is strongly linked to nutrient availability and the physical properties of water masses underlying the food web [Le Borgne *et al.*, 2011]. Mesozooplankton (0.2–2 mm) are consumed by macrozooplankton (2–20 mm) and micronekton (2–20 cm). Micronekton and to a lesser extent macrozooplankton are the prey of top predators such as tuna and other large pelagic fish [Le Borgne *et al.*, 2011]. Knowledge of zooplankton variability is fundamental for oceanic pelagic ecosystem studies aiming to monitor large pelagic fish (e.g., albacore tuna in the Nectalis program) [Menkes *et al.*, 2014]. Such knowledge is poor or lacking in the southwestern Pacific, as the only regions where zooplankton data exist are largely confined to the epipelagic zone in the coastal area of New Caledonia in the Coral Sea (south western lagoon) [Le Borgne *et al.*, 2010] and the coastal waters of the Great Barrier Reef [McKinnon *et al.*, 2005; Young *et al.*, 2011].

Zooplankton sampling coupled with analysis of physical features such as eddies and fronts would contribute to our understanding of the biological and physical factors that control their dynamics. In the

southwestern Pacific, eddy features are ubiquitous and are generated by two major regional processes: (1) to the north of New Caledonia, in the Coral Sea, by barotropic instability generated by the north Caledonian and Vanuatu Jets. (2) South of New Caledonia, in the 20°–30° latitudinal band, due to baroclinic instability of the STCC (Sub Tropical Counter Current) generated by the meeting of two opposite flows: the eastward STCC and the westward South Caledonian Jet [Qiu *et al.*, 2008; Couvelard *et al.*, 2008]. The mesoscale eddy field in the south western Pacific and especially in the STCC region is characterized by an eddy life cycle with three dynamic phases depending on the period of the year: growing (August–October), maturing (November–January) and decaying (March–June) phases [Qiu *et al.*, 2008]. Eddies in the Coral Sea have radii between 25 and 300 km [Couvelard *et al.*, 2008] and they are generated by a complex topography dominated by several islands and reefs initiating nonlinear currents [Gourdeau *et al.*, 2008; Marchesiello *et al.*, 2010].

Eddies have been shown to be a strong driver of surface chlorophyll concentration by horizontal advection in the Southeastern Pacific [Chelton *et al.*, 2011]. In the Coral Sea mesoscale eddies are important features [Suthers *et al.*, 2011] and have the potential to become enriched in phytoplankton [Tranter *et al.*, 1983] and to affect zooplankton assemblages [Griffiths and Brandt, 1983] in the southwestern Pacific off the coast of New South Wales, Australia. The role of such mesoscale feature on secondary productions have been also investigated in other parts of the world ocean; in the Atlantic [e.g., Wiebe *et al.*, 1976; Davis and Wiebe, 1985, Benitez-Nelson and McGillicuddy, 2008], the eastern Pacific off California [Smith and Lane, 1991] and in the Mediterranean Sea [Molinero *et al.*, 2008].

Acoustic sampling is increasingly being used to characterize zooplankton horizontal and vertical distributions. Currently, the available acoustic samplers are either noncalibrated mono-frequency (e.g., ADCP: acoustic Doppler current profiler) or calibrated mono and multifrequency (TAPS: Tracor acoustic profiling system, scientific echosounder, ZAP: zooplankton acoustic profiler). The high temporal and spatial coverage provided by acoustic data enables resolution of small scale phenomena that cannot be resolved with net sampling (eddies, fine scale vertical structures). In addition, acoustic data can augment net sampling that may under sample certain zooplankton size classes, depending on the used mesh size. The primary instruments used for this purpose are scientific echosounders, the ADCP, and the TAPS. Several studies have used scientific echosounders and net systems to examine zooplankton/micronekton assemblages [e.g., Wiebe *et al.*, 1990; Lavery *et al.*, 2010]. ADCPs combined with *in situ* measurements using nets have been used to study variability in zooplankton biomass and diel vertical migration [e.g., Heywood *et al.*, 1991; Zhou *et al.*, 1994; Batchelder *et al.*, 1995; Luo *et al.*, 2000; Jiang *et al.*, 2007; Smeti *et al.*, 2010]. ADCPs sample at a relatively high temporal resolution (e.g., 5 min sampling intervals) and can operate continuously for months if deployed on a mooring line [e.g., Radenac *et al.*, 2010] or for the entire duration of a research cruise in the case of shipborne ADCPs. For example in the Caledonian Exclusive Economic Zone (EEZ), acoustic sampling with shipborne ADCP, a TAPS and a scientific echosounder allowed collection of high resolution acoustic backscatter data during the Nectalis cruises (Nectalis program) [Menkes *et al.*, 2014] complementing net sampling of mesozooplankton.

During the hot and the cool seasons of 2011 two cruises were conducted in the New Caledonian EEZ under the Nectalis programme. The primary objective of these cruises was to reduce the gap in the knowledge of tuna prey spatiotemporal dynamics in the main fishing areas through the study of the mid-trophic levels of the pelagic ecosystem (zooplankton and micronekton) to ultimately better understand the relationship between the albacore tuna (*Thunnus alalunga*), its environment and its fisheries in the EEZ. Meso and macrozooplankton dynamics (abundance, distribution, biomass and composition) are largely unknown in the EEZ and their relationships with the physical environment are poorly understood.

The overall structure of the food web during the Nectalis cruises was described by Menkes *et al.* [2014] based on *in situ* measurements of hydrodynamic parameters, nutrients, phytoplankton, primary production, and the biomass of zooplankton and micronekton. They showed a clear seasonal difference in the coupling between the ocean dynamic and the biological components for the low trophic levels (phytoplankton), and little difference for the midtrophic levels (zooplankton and micronekton), probably due to different turnover times and delay in transmission of the primary production to the upper trophic levels. These authors showed that the sampling techniques (net and acoustics) of zooplankton and micronekton compared reasonably well.

In this paper we focus on the analysis of the spatial and seasonal variability of zooplankton (abundance, distribution, biomass and taxonomic composition) and its relationships with mesoscale features (eddies and fronts) and trophic variables (chlorophyll and nutrients). We also focus on the inter-comparability of the zooplankton sampling techniques used (net and acoustics). Finally we consider the application of acoustic techniques (with a focus on shipborne ADCP) to improve and promote collection of high frequency estimates of zooplankton distribution in future studies, especially in highly dynamic regions where the mesoscale activity is intense (e.g., the EEZ of New Caledonia).

2. Methods

2.1. Sampling Strategy

The Nectalis cruises were conducted on board of R/V Alis (IRD, Nouméa) during two contrasted seasons, from 29 July to 16 August 2011 (cool season) and from 26 November to 14 December 2011 (hot season). The location and timing (day/night) of the sampling stations are presented in Figure 1. The two surveys broadly followed the same track with some variations due to weather.

2.2. Physical Environment

2.2.1. In Situ Measurements

Temperature and salinity were measured at all stations using a CTD coupled with a 10 Niskin bottles rosette that was lowered to ~500 m depth. Surface temperature (SST) and salinity (SSS) was recorded continuously with thermosalinograph for the entire duration of each cruise. Further details about the in situ sampling of physical parameters could be found in *Menkes et al.* [2014].

2.2.2. Satellite Data

Net primary production (NPP), geostrophic current (GC), sea level anomaly (SLA), sea surface temperature (SST) and Finite Size Lyapunov Exponent (FSLE) were extracted along Nectalis cruises ship track. NPP is based on MODIS satellite data and Vertically Generalized Production Model (VGPM) (www.science.oregon-state.edu/ocean.productivity/). GC was extracted from the Ocean Surface Current Analysis (OSCAR, www.oscar.noaa.gov) satellite-derived data set at a resolution of 1/3° and 5 day. Cyclonic and anticyclonic eddies were identified from sea level anomaly (SLA) maps with cyclonic and anticyclonic eddies having positive and negative SLA, respectively. SLA was extracted from the AVISO data set derived from satellite altimeter (www.aviso.oceanobs.com/en/data/products/sea-surface-height-products/global/msla.html#c5122) at a resolution of 1/3° and 7 days. Daily SSTs were obtained from the Group for High Resolution SST (GHRTTS, www.ghrsst.org) at a 1/12° grid resolution. Formally, the Lyapunov exponent λ characterizes the time scale of divergence of a fluid, as expressed in equation (1) where δ_0 is the smallest separation distance between two water-masses and δ is the final separation distance between the same water-masses after a time t of advection. The FSLE computes λ while defining the spatial scale by setting δ_0 and δ to constant values. Here the method is used backward in time, i.e., computing λ from the negative time t necessary to enlarge the separation distance of water-masses from δ_0 to δ , which is equivalent to characterize the convergence time scale of water-masses forward in time. Hence, λ has a negative value. High values of $|\lambda|$ indicate a rapid concentration of the fluid at filament scales and a null value of $|\lambda|$ would indicate no fluid concentration. For a more detailed description of the FSLE computation method one should refer to *D'Ovidio et al.* [2009, 2013]. Mean FSLE maps during the Nectalis cruises were computed from daily FSLE data with $\delta_0=1/25^\circ$ and $\delta=0.6^\circ$, using a linear interpolation of the geostrophic currents extracted from global AVISO MADT weekly products with spatial resolution of 1/3° (<http://www.aviso.altimetry.fr/en/data/products/sea-surface-height-products/global/madt.html>, 2012 processing). The maximum time of advection is limited to 200 days after which, if the distance $\delta=0.6^\circ$ has not been reached, λ is set to null value.

$$\lambda = \lim_{t \rightarrow \infty} \lim_{\delta_0 \rightarrow 0} \frac{1}{t} \ln \frac{\delta}{\delta_0} \quad (1)$$

NPP data were used to describe the variations of surface primary production along the Nectalis cruises ship-track and its relationship to surface zooplankton biomass distribution. Geostrophic current and SLA data were used to identify mesoscale eddies that were present during the in situ sampling. FSLE was used to investigate the influence of fronts on zooplankton biomass measured at Nectalis stations. Local maxima of FSLE (ridges) can be used to predict accumulation of tracers (e.g., phytoplankton, zooplankton) at fronts

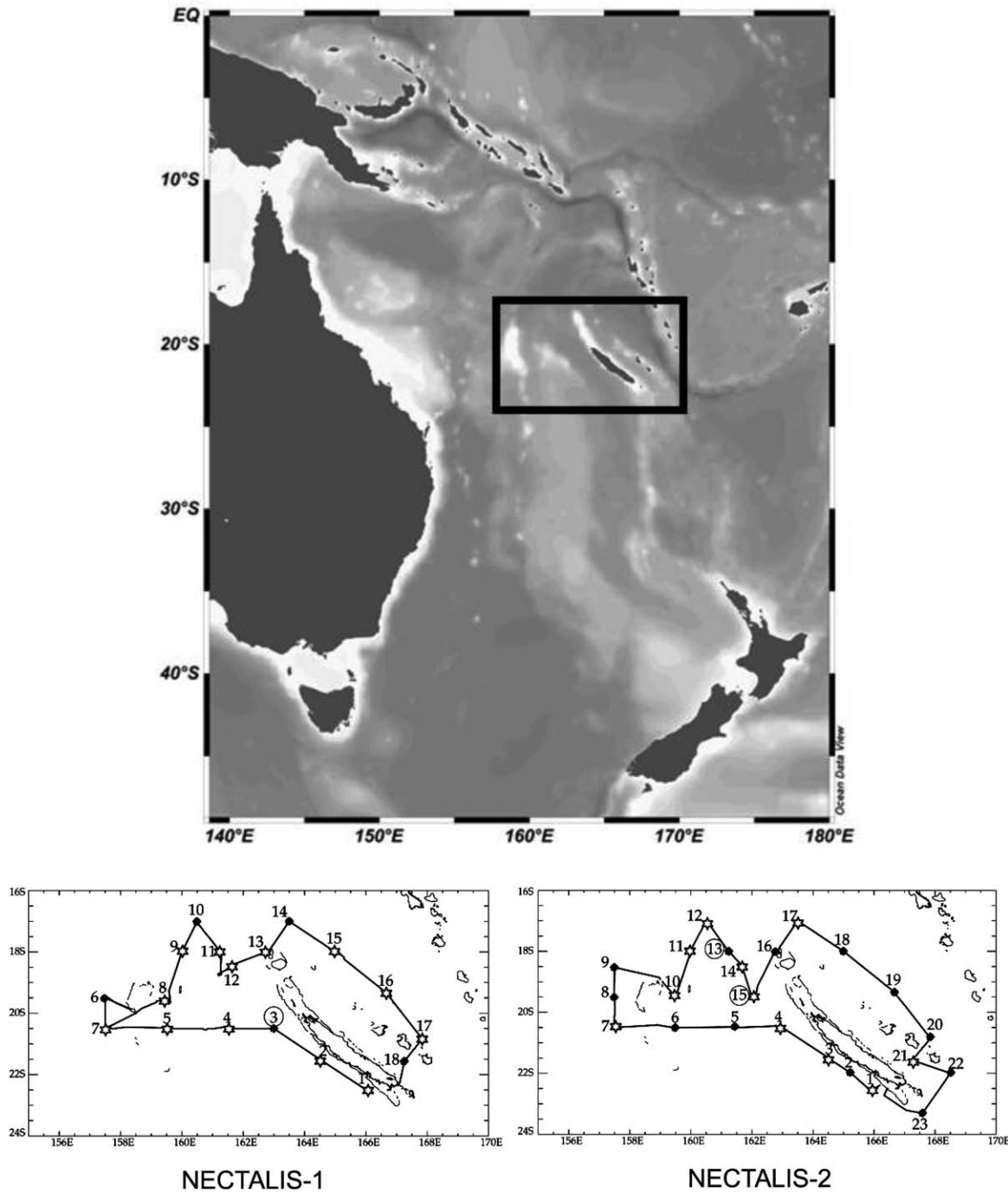


Figure 1. (top) The Southwestern Pacific region (adapted from *Hunt et al.* [2014]) where the Nectalis program took place in the Caledonian Exclusive Economic Zone (black rectangle). (bottom) NECTALIS cruises ((left) Nectalis 1 in July 2011; (right) Nectalis 2 in November 2011) and associated stations. The black solid lines shows the ship track; the star symbols show day-time stations; filled circles show night-time stations. Station numbers surrounded with a circle means there was no zooplankton sampling with the Multinet.

(e.g., filaments and frontal regions of eddies) induced by passive horizontal stirring caused by altimetry-derived mesoscale velocities [*D'Ovidio et al.*, 2004]. The values of FSLE along the ship track were used for correlation with ADCP-derived zooplankton biomass to assess the importance of frontal aggregation of zooplankton. The eddy depiction index (Okubo-Weiß parameter) was used to examine the surface ocean dynamics using an eddy detection algorithm following the method described in *Menkes et al.* [2014].

Table 1. Zooplankton Sampling Methods During the NECTALIS Surveys

Sampling Technique	TAPS	Multinet	ADCP	Echosounder
Size range detected	Equivalent radius 0.05–3 mm	Length 0.2 to few mm	Length few mm to few cm	Length ~2 mm to few cm
Most representative groups	Microzooplankton to mesozooplankton	Mesozooplankton to macrozooplankton	Macrozooplankton to micronekton	Macrozooplankton to micronekton
Depth range	20–180 m	0–600 m	16–104 m	16–104 m
Vertical resolution	2 m	100 m	8 m	8 m

2.3. Chemistry and Phytoplankton

Chlorophyll-a (Chla), ammonium, phosphate, nitrate and nitrite concentrations were measured in water samples collected from Niskin bottles in the upper 200 meters at the Nectalis cruises sampling stations and were used to test for correlation with zooplankton biomass estimators. A detailed description of sampling methods and measurement protocols can be found in *Menkes et al.* [2014].

2.4. Zooplankton

A large range of zooplankton size classes was sampled by combining net and acoustic sampling. Table 1 presents zooplankton sampling techniques used during the Nectalis program.

2.4.1. Net Tow

Mesozooplankton (200–2000 μm in length) were collected with an Hydrobios MultiNet (Kiel, Germany), equipped with five 200 μm mesh nets. We sampled 5 layers of the water column from the surface to 600 m depth (0–100, 100–200, 200–400, 400–500, 500–600 m). Each net was equipped with a mechanical Hydrobios flowmeter. Volume filtered by the nets was calculated from the flowmeter counts and the mouth area of the net (0.25 m^2). The formula used to calculate the filtered volume is $V = K * R * S$; where $K = 0.3$ m/revolution is the pitch of the impeller of the flowmeter provided by the manufacturer; R = number of revolutions of the flowmeter; $S = 0.25$ m^2 is the surface area of the net mouth. Zooplankton was collected during day and night stations. During Nectalis-1, 13 day-time and 4 night-time tows were collected, while 10 day-time and 11 night-time tows were collected during Nectalis-2. Samples from stations 3 (Nectalis-1) and 13, 15 (Nectalis-2) were discarded due to technical problems with the Multinet.

2.4.1.1. Dry and Wet Weights

Samples from net tows were immediately preserved in a 5 % buffered formalin-seawater solution. At the end of the cruise, in the on shore laboratory, samples from the 0–100 and 100–200 m layers were split using a Folsom splitter [*Harris et al.*, 2000]. One half-split was kept for dry weight analysis and the other half for wet weight, taxonomic identification and ZooScan analyses. Due to the low biomass in the 200–400, 400–500, and 500–600 m layers, these samples were not split and entirely kept for wet weight, taxonomic and ZooScan analyses. Thus dry weight was measured over the first 200 m of the water column and wet weight over all 5 layers sampled with the Multinet. The subsamples for dry weight measurement were filtered onto preweighed GF/F filter then rinsed with distilled water to remove formalin and salt and dried in the oven at 60°C for 72 h. The dry samples were weighed on a Precisa 405M-200A micro-balance (precision 0.01 mg) and the biomass was expressed in mg dry weight m^{-3} (DW) [*Harris et al.*, 2000]. The subsamples for wet weight were sieved onto preweighed circle nylon gauzes (47 mm diameter, 100 μm mesh size), rinsed with distilled water, blotted on absorbent paper and weighed immediately. The biomass was calculated in mg wet weight m^{-3} (WW). After the weighing, the zooplankton on the gauze was re-transferred in the 5% buffered formalin solution for further microscope counts, identification and ZooScan analyses.

2.4.1.2. Identification and Counts

Taxonomic identification and counts of zooplankton from the 0–100 m layer were done using a LEICA MZ6 dissecting microscope. Very common taxa were counted in subsamples (1/32 or 1/64), and the whole sample was examined for either rare species and/or large organisms (i.e., euphausiids, amphipods). Identification of the copepods community was made down to species level and developmental stage when possible. Species/genus identification and size estimation of each taxa were made according to *Trégouboff and Rose* [1957] and *Razouls et al.* [2005–2014]. The diversity of the zooplankton was determined using the Shannon-Weaver index [*Shannon and Weaver*, 1949].

2.4.1.3. Digital Imaging Approach With the ZooScan (Abundance and Biomass)

After homogenization, a fraction of each preserved sample containing a minimum of 1000 particles was placed on the glass plate of the ZooScan. Organisms were carefully separated one by one manually with a wooden spine, in order to avoid overlapping. Each image was then run through ZooProcess plug-in using the image analysis software Image-J [Grosjean *et al.*, 2004; Gorsky *et al.*, 2010]. Several measurements of each organism were then computerized. Organism size is given by its equivalent circular diameter (ECD) and can then be converted into biovolume, assuming each organism is an ellipsoid [see Grosjean *et al.*, 2004]. The lowest ECD detectable by this scanning device is 300 μm . To discriminate between aggregates and organisms, we used a training set of about 1000 objects which were selected automatically from 39 different scans. Each image was classified manually into zooplankton or aggregates and each scan was then corrected using the automatic analysis of images.

The formula used to convert the area (*Area*) measured by the software ZooProcess to biovolume is presented in equation (2):

$$BioV = \frac{4}{3} \times \frac{Area}{\sqrt{Ratio}} \times \sqrt{\frac{Area}{\pi}} \quad (2)$$

where *BioV* is the biovolume in $\text{mm}^3 \text{m}^{-3}$; Ratio is the ratio between the major and minor axes of the prolate spheroid corresponding to the body of an individual. We assumed a ratio of 3 considering the dominance of copepods in our samples [Espinasse *et al.*, 2012]. To convert biovolume to biomass in WW, the density of 1 mg WW mm^{-3} was used for zooplankton [Wiebe *et al.*, 1975].

2.4.2. Mono-Frequency Acoustic

A shipborne broadband 153 kHz Acoustic Doppler Current Profiler (Teledyne-RDI, California) mounted on the R/V Alis was used to obtain profiles of horizontal current (U-ADCP, V-ADCP) speed and acoustic backscatter from 15 to 150 m. ADCP profiles were recorded over 40 vertical bins with a profiling interval of 5 min (5 min average) and a bin size of 8 m. During the transit between the sampling stations the ship was streaming at a speed of ~ 7 knots so that the distance covered by the 5 min averaging of the ADCP data is ~ 1080 m. The zooplankton scatterers that are most likely to be detected at 153 kHz have a size range of a few millimeters to a few centimeters [Sutor *et al.*, 2005]. Luo *et al.* [2000] proposed that the scatterers detected by a 153 kHz ADCP has a minimum ESD of ~ 1 mm. However, Mutlu [2003], based on the works by Wiebe *et al.* [1990] and David *et al.* [1999] suggest that the minimum size would be about 2 mm at 200 kHz. Hence, in this paper we use backscatter data from 153 kHz ADCP to target zooplankton in the size range of a few millimeters to few centimeters (mostly macrozooplankton) that are under-sampled by the Multinet and the TAPS that target both part of micro and the mesozooplankton (50–3000 μm in ESR).

The echo intensity recorded by the ADCP (counts) is converted to backscatter coefficient using the equation given by Deines [1999] and rearranged by Gostiaux and van Haren [2010] as presented in equation (3):

$$S_V = C + 10 \log_{10} [(T_x + 273.16)R^2] - L_{DBM} - P_{DBW} + 2\alpha R + 10 \log_{10} \left[10^{K_c E / 10} - 10^{K_c E_{noise} / 10} \right] \quad (3)$$

where S_V is the volume backscattering strength in dB re $(4\pi \text{ m})^{-1}$. C is an empirical constant required to account for some of the relevant phenomena affecting echo intensity that cannot be measured independently. T_x is the temperature of the transducer ($^{\circ}\text{C}$) and R is the depth along the beam to the scatterers (m). L_{DBM} is $10 \log_{10}$ (transmit pulse length, meters) and P_{DBW} is $10 \log_{10}$ (transmit power, Watts). α is the sound absorption coefficient of water ($\text{dB}\cdot\text{m}^{-1}$). K_c is the conversion factor for echo intensity (dB count^{-1}). E is the ADCP raw echo intensity (counts) and E_{noise} is the reference level of E . For every ADCP profile we assumed E_{noise} to be the lowest value (at the end of the profile) of the 4 beams average of E [Deines, 1999; Jiang *et al.*, 2007; Radenac *et al.*, 2010].

Contact with RDI was made to obtain C , P_{DBW} and K_c . These instrument-specific characteristics are recorded at the factory by the manufacturer for every beam [Deines, 1999]. However, RDI is no longer supporting Broadband 153 KHz ADCPs (personal communication of Gregory Rivalan, Teledyne RDI). Hence the calculation of S_V did not take into account the actual RV-Alis' ADCP specificities and C , P_{DBW} and K_c values were taken from the literature [Deines, 1999] which led to compute and use a relative volume backscattering strength (S_V).

Due to technical constraints related to ship-mounted ADCP there was no specific calibration of the ADCP backscatter with major groups of zooplankton scatterers following *Stanton et al.* [1994] classification: gas-bearing (e.g., siphonophores), fluid-like (e.g., euphausiids) and hard elastic-shelled (e.g., pteropods). Hence, the ADCP-derived biomass used in this study is a relative acoustic estimate of zooplankton biomass mostly dominated by large zooplankton species or small gas bearing organisms.

For each sampling station ADCP backscatter data were depth-averaged over nominally ~16–104 m (this depth range may vary by \pm few meters depending on sea conditions), then time-averaged over 20 min (10 min before and 10 after the timing of net tows). Before averaging, Sv data were transformed to a linear scattering measure ($10^{Sv/10}$).

Zooplankton DW from net tows (0–100 m) was used for regression with ADCP backscatter (Sv, 16–104 m.) to estimate ADCP-derived biomass from relative backscatter data applying the following calibration formula: $Sv = \alpha \times \log_{10}(DW/4\pi) + \beta$, where Sv is the relative backscattering strength; DW is zooplankton dry weight from net tows. $\alpha = 7.4$ and $\beta = -79.4$ are the slope and intercept of the regression equation. Sv and $\log_{10}(DW/4\pi)$ were normally distributed (Saphiro-Wilkinson test; $p > 0.05$).

From the regression equation the acoustically estimated biomass was calculated as:

$$B_{ADCP} = 10^{\left(\frac{Sv}{7.4} + 10.7\right)} \times 4\pi; \quad r = 0.51, \quad p < 0.001, \quad n = 38$$

Where B_{ADCP} is the estimated zooplankton biomass ($\text{mg dry mass} \cdot \text{m}^{-3}$) from ADCP; Sv is the relative backscattering strength in dB $(4\pi \text{ m})^{-1}$. r is the correlation coefficient, p is the significance level for the regression and n is the number of samples used in the regression.

2.4.3. Multifrequency Acoustic

A Tracor Acoustic Profiling System (TAPS-6, BAE Systems, San Diego, CA, USA) operating at six frequencies (265, 420, 710, 1100, 1850, 3000 KHz) was used to derive at every sampling station the biovolume (Bv, 6–180 m.) of zooplankton in the size range of 0.05–3 mm [*Holliday and Pieper*, 1995] of equivalent spherical radius (ESR) (Table 1). The TAPS was therefore used to estimate zooplankton biovolume taking into account the small most numerous zooplankton in the tropical seas [*Holliday and Pieper*, 1995; *Ceccarelli et al.*, 2013]. The TAPS was operated in “cast mode”, profiling the water column in horizontal position, ensonifying a volume of ~5 l at each ping [*Pieper et al.*, 2001]. The volume-backscattering strength (Sv, in dB) recorded by the TAPS-6 was transformed into biovolume estimates using an inversion algorithm following the method described in *Lebourges-Dhaussy et al.* [2014]. Bv estimates were obtained for different size classes (0–0.2, 0.2–0.4, 0.4–1, 1–1.6, 1.6–2.3, >2.3 mm) then grouped into total Bv, $Bv < 1.6$ mm (small zooplankton) and $Bv > 1.6$ mm (large zooplankton).

2.4.4. Split-Beam Echosounder

A hull-mounted EK60 echosounder (SIMRAD Kongsberg Maritime AS, Horten, Norway) was used to collect continuous (concurrent) acoustic data on the abundance of mesozooplankton (mainly copepods, Multu, 2003) from the near surface (~5 m) to ~100 m depth using the 200 kHz transducer. The EK60 signal was processed [*Menkes et al.*, 2014] to obtain volume backscattering strength (Sv) data [*MacLennan et al.*, 2002] for comparison with the Sv from the ADCP available for roughly the same layer (16–104 m). The EK60 was calibrated before each cruise and the computed Sv data are absolute values, unlike the noncalibrated ADCP that only provides relative Sv values. At station, the EK60 200 kHz data were not usable due to the contamination of the signal by the flow noise and air bubbles, so that we were not able to perform a regression analysis between the EK60Sv and zooplankton biomass from net tows. Hence, we use the EK60 absolute Sv data as a proxy of small zooplankton abundance.

2.5. Statistical Methods

For statistical analysis we used zooplankton biomass and abundance data from the upper 100 m of the water column, to compare with population composition data that are available only for the surface layer. Spearman's rank correlation coefficients (Rs) were calculated to compare the zooplankton biomass and abundance estimators derived from the different methods (net and acoustics).

Two-way analysis of variance (ANOVA) was used to test for the effects of the seasons (Nectalis-1/Nectalis-2) and time of the day (day/night) (and their interactions) on the environmental variables and the zooplankton estimators. ANOVA were performed on log-transformed data to tend toward variance normality. The non-parametric rank-sum Mann-Whitney test (U test) was performed when normality was not reached (according to the Saphiro-Wilkinson test).

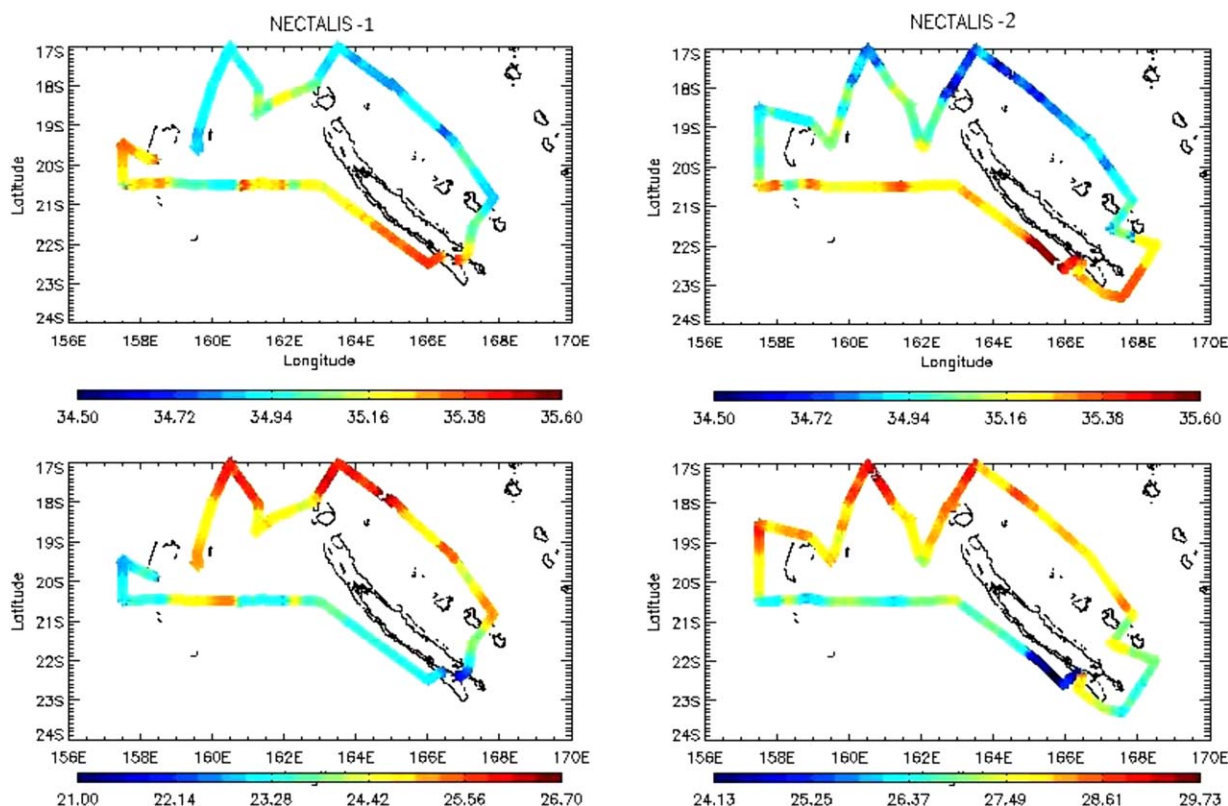


Figure 2. (top) Sea surface salinity SSS and (bottom) sea surface temperature SST (°C) from ship sensors during (left) Nectalis-1 and (right) Nectalis-2.

Spearman’s rank-correlation (R_s) were computed to test relationships between continuous ADCP-derived zooplankton biomass (along the ship track) and environmental parameters (longitude, latitude, SST, SSS, U-ADCP, V-ADCP, FSLE, Chla, NPP). In order to test for coherence patterns between the ADCP-derived biomass and the SST cross-correlation (R_{xy}) and coherence analyses (C_{xy}) were applied.

The spatial variation of the zooplankton community composition was investigated using multivariate analysis, specifically Nonmetric Multidimensional Scaling (NMDS). A species by station matrix was created for abundance data. The abundance data were square root transformed before estimation of station similarity using the Bray Curtis metric. The similarity matrix was then ordinated using NMDS. A SIMPER (percentage of similarity) analysis was performed to identify the species contributing most to similarity within stations and dissimilarity between stations for the station groupings identified by NMDS.

Finally to investigate what environmental variables were most strongly related to community composition, we used a multiple linear regression in which the first two dimensions of the NMDS analysis are the independent variables while the environmental variables are considered the dependent variables [Hosie and Cochran, 1994]. The environmental variables used are the longitude, latitude, SSS, SST, Chla, the concentration pheopigments, maximum concentration of Chla, maximum concentration of pheopigments, ammonium, phosphate, nitrate and nitrite.

3. Results

3.1. Physical Environment

3.1.1. Temperature and Salinity

During Nectalis-1 (cool season) two distinct regions were identified with the hydrographic data. The north of the EEZ, north of $\sim 20^\circ\text{S}$ (from station 8 to 17) was characterized by warm and fresher waters while the southern part had colder and saltier waters (Figure 2). A strong temperature and salinity gradient was seen

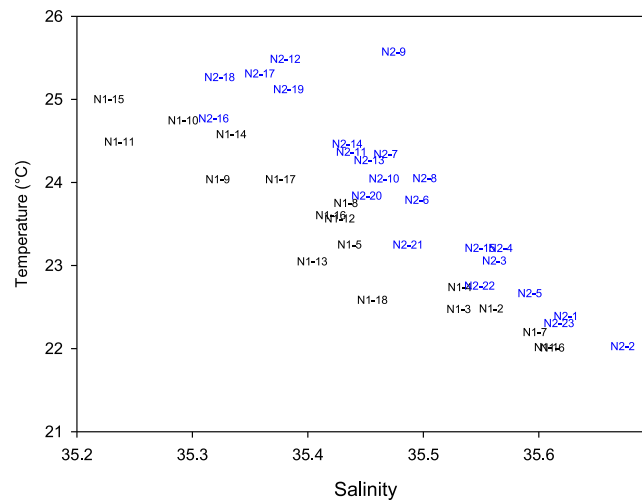


Figure 3. TS-diagram (temperature and salinity averaged over 0–100 m). Stations ID are represented: Nectalis-1 (N1, black) and Nectalis-2 (N2, blue).

between the northern and southern parts of the survey area with a well established frontal region centered around 19–20°S, as evidenced by satellite-derived SST [Menkes *et al.*, 2014]. During Nectalis-2 (hot season) the same gradient was observed, but was weaker, with a warming of surface waters by ~2°C and a greater penetration of the warm waters southward (Figure 2).

Both the spatial and seasonal variation of temperature and salinity are well represented by the TS diagram where the data from the two cruises are clearly separated (Figure 3). In both

cruises, southern waters were colder and saltier (stations with temperature ~< 23.5°) and waters to the north warmer and fresher (stations with temperature ~> 23.5°). Seasonally, during Nectalis-2, higher temperature was recorded, typical of the hot season with a greater penetration of the warm and fresh waters southward [Menkes *et al.*, 2014].

3.1.2. Mesoscale Activity

The eddy activity in the Coral Sea off New Caledonia is important with cyclonic and anticyclonic eddies present during both cruises with a more intense activity during Nectalis-2 (Figure 4). The diameter of eddies that were present in the EEZ during the Nectalis cruises was on average between 100 and 200 km (Figure 4). The mesoscale aspect of the circulation in the EEZ and its potential impact on the biogeochemistry is discussed in Menkes *et al.* [2014]. Four eddies were sampled during the Nectalis cruises: two cyclonic eddies during the cool season (Nectalis 1) at stations 6 and 10, and two anticyclonic eddies during the hot season (Nectalis 2) at stations 7 (periphery) and 9 (center); these later eddies had stronger signature on the SLA maps (Figure 4). The position of these eddies at the sampling dates were determined using daily FSLE maps (not shown). These maps also allowed to locate stations 12 and 13 (Nectalis-1) at the limit of a tight front. Maps of FSLE averaged over cruise periods showed clearly the importance of submesoscale (filaments) and mesoscale (periphery of eddies) fronts (Figure 4).

3.2. Primary Production

Satellite-derived net primary production (NPP) was tightly related to sea surface temperature (SST) during Nectalis-1 ($R_s = -0.87$, $p < 0.0001$) with higher NPP (ANOVA; $p < 0.05$) in the south-western (SW) part of the survey area (stations 1–7), characterized by colder and saltier waters (Figure 5a). These high NPP waters were characterized by relatively low SST (ANOVA; $p < 0.05$) with mean station NPP value of $368 \text{ mgC m}^{-2} \text{ d}^{-1}$ (average Nectalis-1 NPP = $296 \text{ mgC m}^{-2} \text{ d}^{-1}$). In the north-eastern (NE) part of the survey area (stations 8–18), waters were warmer and NPP was on average lower with mean station value of $250 \text{ mgC m}^{-2} \text{ d}^{-1}$. The NE-SW strong difference in NPP observed during Nectalis-1 was not seen during Nectalis-2 and there was no significant correlation between NPP and SST ($p >> 0.05$) during Nectalis-2. Average station NPP during Nectalis-2 was $197 \text{ mgC m}^{-2} \text{ d}^{-1}$ (Figure 5b).

3.3. Zooplankton

3.3.1. Methods' Comparison

Overall, all correlations between zooplankton biomass or abundance estimates were significant, with the exception of the relationships between TAPS biovolume of the small fraction ($\text{ESR} < 1.6 \text{ mm}$) and the Multinet-derived abundance and the ZooScan-derived abundance and biomass (Table 2). The strongest correlations were between the zooplankton total abundance, DW and WW parameters derived from the

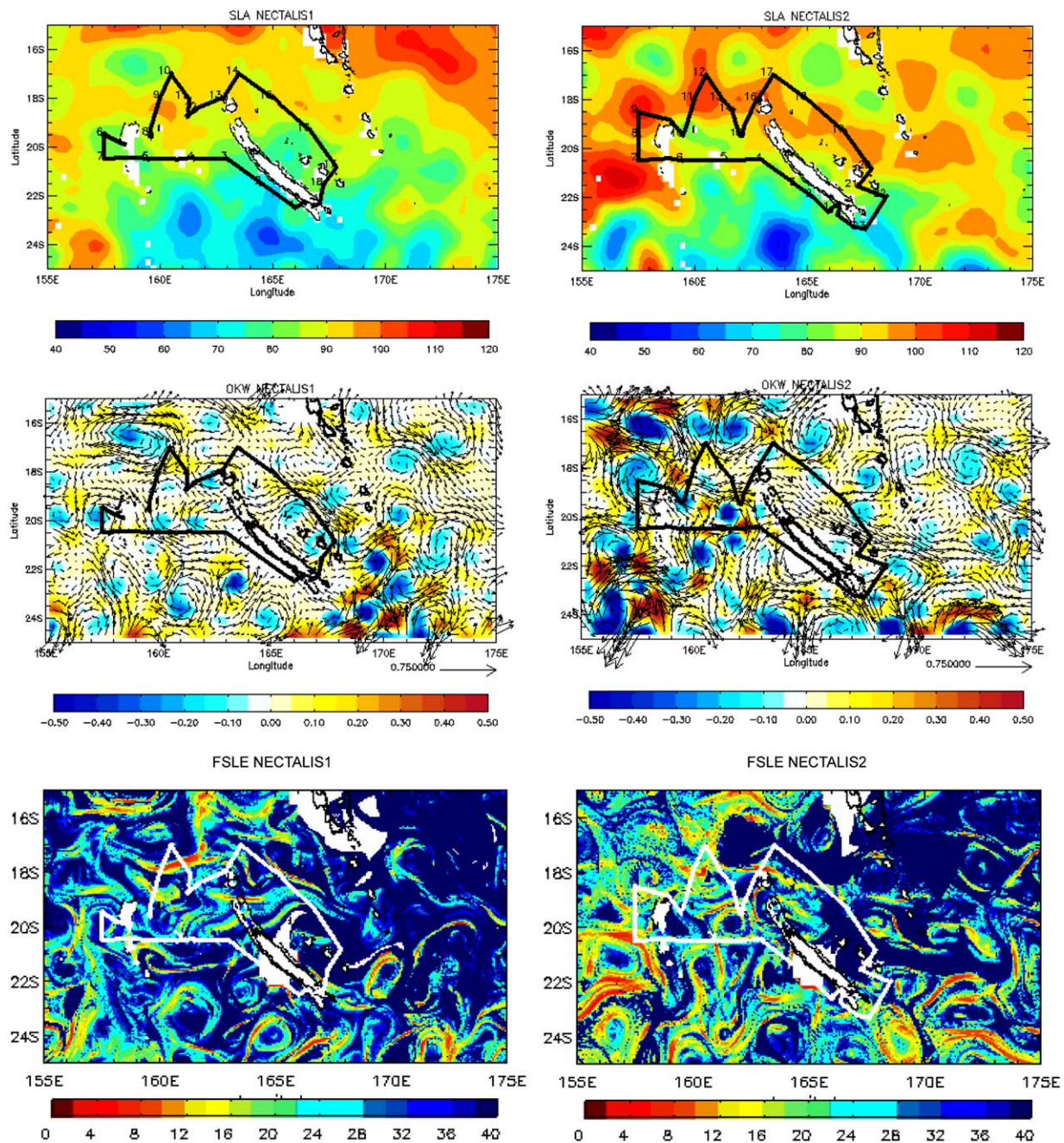


Figure 4. Contours of (top) sea level anomalies (SLA, color scale in cm), (middle) eddy depiction index Okubo-Weiß parameter (OKW, color scale in day^{-2}) with an overlay of satellite-derived surface current vectors. SLA and OKW contours are adapted from Menkes et al. [2014]. (bottom) Mean FSLE during the Nectalis cruises, color scale in day^{-1} . (left) Nectalis-1 and (right) Nectalis-2. Cruise tracks are plotted as black solid lines in top and middle rows and as white solid lines in bottom row.

Multinet ($R_s \geq 0.8$, $p < 0.001$; Table 2). The ZooScan-derived biomass of the larger fraction (>1.6 mm) was better correlated with the ADCP or TAPS derived biomass than the smaller fraction (<1.6 mm).

The comparison of mean biomass values obtained from the different methods (Figure 6) showed a good agreement between the DW from Multinet and B_{ADCP} . A good correlation ($R_s > 0.5$, $p < 0.001$) was found between the wet biomass from Multinet and ZooScan. Overall, both instruments gave the same magnitude of biomass with slightly lower values obtained with the ZooScan. The size of the organisms detected with the zooscan ranged between 300 and 3000 μm (ESD) in both cruises. The mean individual size per station ranged between 600.1 μm and 789.9 μm of ECD during Nectalis 1 (mean = 690 ± 56.5 μm) and between 560.9 μm and 804.2 μm during Nectalis 2 (mean = 636.5 ± 51.6 μm), with a significant difference between

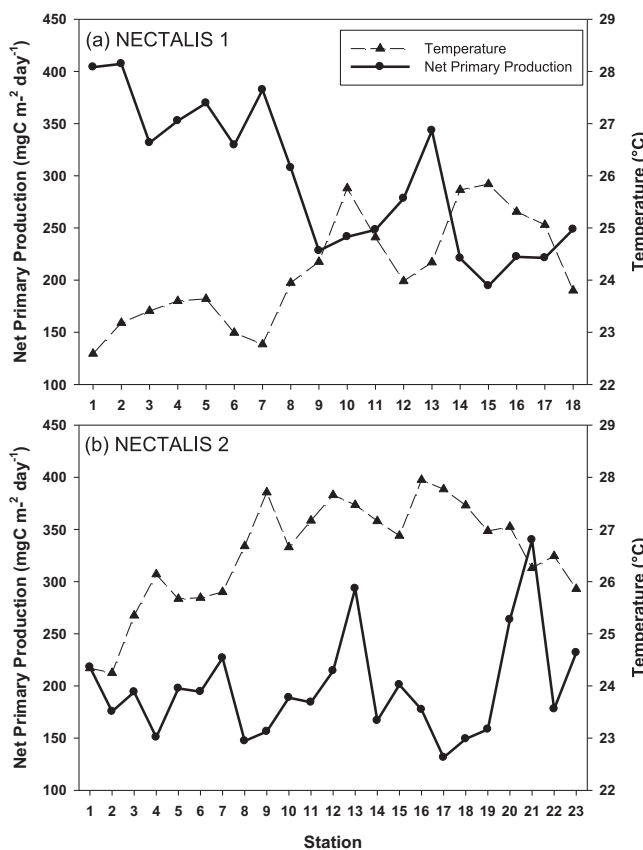


Figure 5. Satellite-derived sea surface temperature (SST) and net primary production (NPP) during the Nectalis cruises.

the two cruises ($p < 0.001$). The ratio between the DW (net weighing) and WW (net weighing and ZooScan estimate) was in agreement with the 10% ratio generally accepted [Harris et al., 2000]. The WW from TAPS (biovolume) overestimated the biomass by one order of magnitude compared to the other methods. If the entire size range detected by the TAPS is considered. But according for example, to the size range mentioned above for the ZooScan processing, the sizes that are expected to be common to the TAPS and to the samples provided by the Hydrobios, and thus that are to be considered for a comparison with the nets results, should more probably be restrained to the classes from 0.2 to 1.6 mm in ESR. In this case, the mean biovolume estimated by the TAPS is about two fold the WW (Figure 6)

The volume backscattering strength (Sv) obtained from the continuous ADCP and EK60 data (only during the transit between stations) were highly correlated in the first ~100 m (Figure 7a). These correlation coefficients decreased below 100 m. Hence, we considered only the mean ADCP and EK60 values for the 16–104 m stratum which were highly correlated and displayed the same variation patterns during both cruises (Figures 7b–7d). The mean Sv values of ADCP and EK60 were -76.2 ± 3.2 dB for and -74.8 ± 3.5 dB, respectively, considering only concurrent values ($n=4209$, paired t test: $p < 0.001$).

3.3.2. Abundance and Biomass
3.3.2.1. Vertical Biomass Distribution

Zooplankton wet weight profiles from the Multinet and the TAPS showed that biomass decreased with depth during both Nectalis cruises (Figures 8a–8c). Most of the zooplankton was located in the upper 100 m layer, where 50–60% of Multinet and 70–80% of TAPS-derived wet weights were found. Multinet

Table 2. Spearman Rank Correlation Coefficients (Rs) Between Different Zooplankton Biomass and Abundance Estimators^a

	(1)	(2)	(3)	(4)	(5)	(6)	(7)	(8)	(9)	(10)
(1) Sv ADCP										
(2) Biovolume (Bv) total TAPS	0.62***									
(3) Bv TAPS >1.6 mm	0.63***	0.86***								
(4) Bv TAPS <1.6 mm	0.37*	0.74***	0.37**							
(5) Dry weight	0.52***	0.52**	0.55***	0.34*						
(6) Wet weight	0.41**	0.50**	0.46**	0.33*	0.80***					
(7) Abundance Multinet	0.40**	0.44**	0.53***	0.17ns	0.82***	0.88***				
(8) Biomass zooscan total	0.49**	0.36*	0.35*	0.25ns	0.58***	0.61***	0.53***			
(9) Biomass zooscan <1.6 mm	0.39*	0.32*	0.33*	0.22	0.51***	0.57***	0.56***	0.92***		
(10) Biomass zooscan > 1.6 mm	0.48**	0.34*	0.28	0.27	0.51***	0.55***	0.41**	0.89**	0.67***	
(11) Abundance zooscan	0.49**	0.34*	0.42**	0.11ns	0.48**	0.54***	0.63***	0.79***	0.85***	0.59***

^aPooled values of the two cruises, $n=38$. Level of significance of the correlation: *** $p < 0.001$, ** $p < 0.01$, * $p < 0.05$, ns = $p > 0.05$.

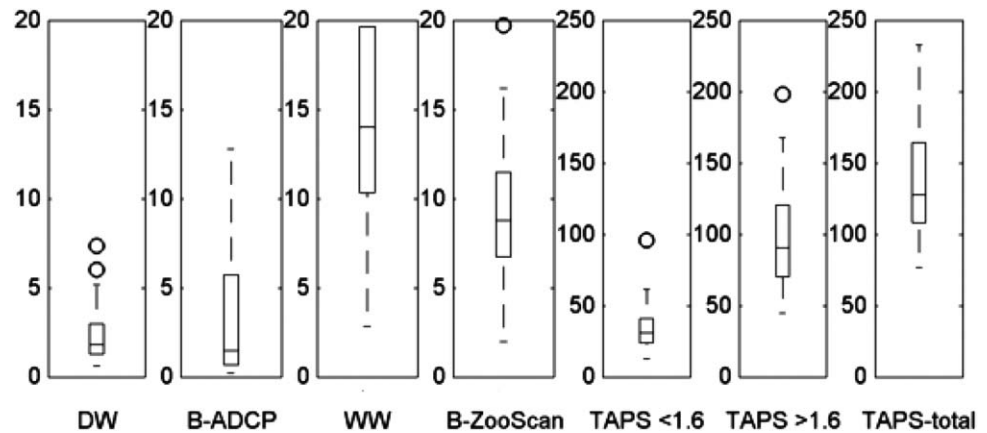


Figure 6. Box plots of zooplankton biomass estimators (0–100 m layer data) for the ensemble of Nectalis-1 and Nectalis-2 data. The y axes represent the biomass in mg m^{-3} . DW=dry weight; B_{ADCP} = biomass (as dry mass) estimated from ADCP at Nectalis stations; WW=wet weight; B-ZooScan = biomass (as wet mass) from the ZooScan; $\text{TAPS} < 1.6$ = TAPS biomass for size classes < 1.6 mm (assimilated to meso-zooplankton); $\text{TAPS} > 1.6$ = TAPS biomass (as wet mass) for size classes > 1.6 mm (assimilated to macrozooplankton); TAPS-total = total biomass from TAPS for all size classes. The box plots denote mean values and 25% and 75% interquartiles ((IQ25 and IQ75 respectively); the whiskers represent $\text{IQ}25 + 1.5$ ($\text{IQ}75 - \text{IQ}25$) and $\text{IQ}75 + 1.5$ ($\text{IQ}75 - \text{IQ}25$); open circles are outliers.

biomass strongly decreased in the 100–200 m layer, and below 200 m biomass was $\sim 27\%$ of the total. Therefore, most zooplankton appeared to be concentrated above the DCM and the thermocline during both seasons (Figures 8d and 8e). The DCM was located around 100 m depth during both seasons with higher chlorophyll concentration at the DCM during Nectalis-2 (U test, $p = 0.0005$; maximum value = $0.35 \mu\text{g L}^{-1}$ during Nectalis-2 and $0.27 \mu\text{g L}^{-1}$ during Nectalis-1). Two maxima of zooplankton biomass were

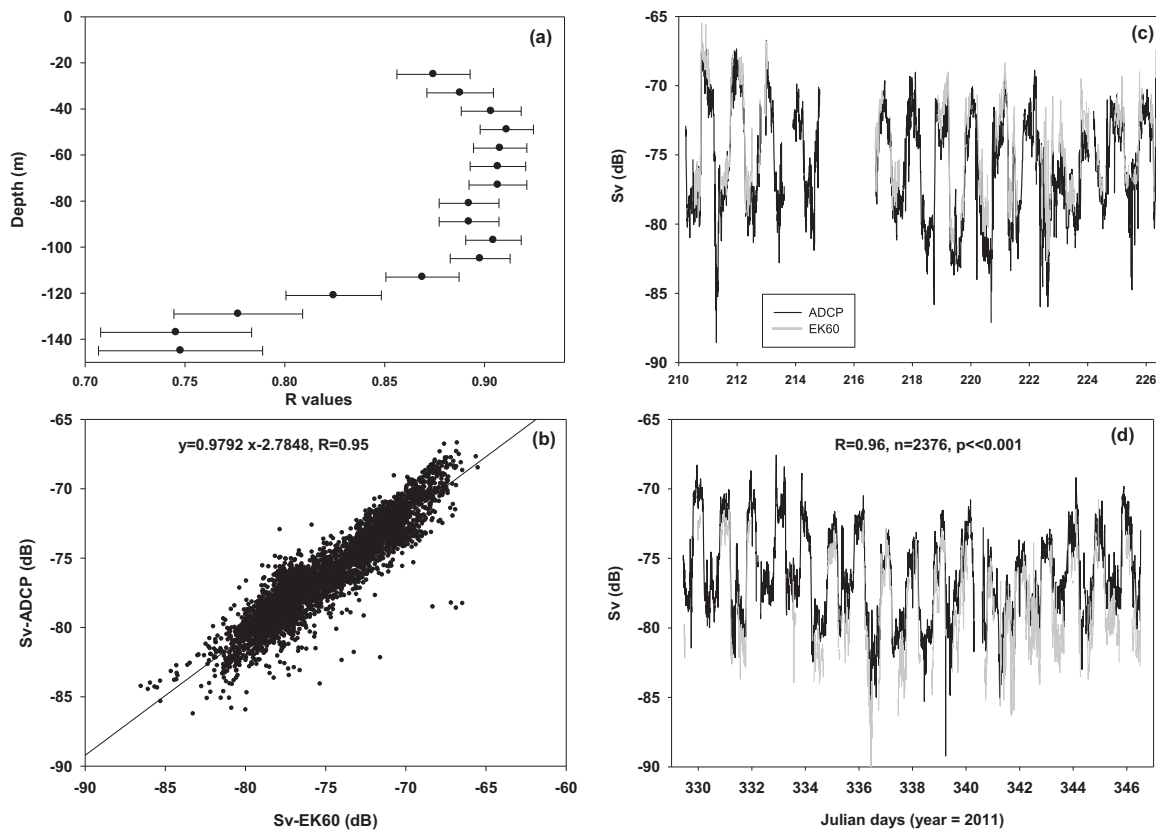


Figure 7. Variation with depth of the (a) mean correlation coefficients between Sv-ADCP and Sv-EK60, (b) scatter plot of the ensemble (ADCP and EK60) Sv data during both Nectalis cruises and variations of mean (16–104 m) Sv values from continuous ADCP (black lines) and EK60 –200 MHz (gray lines) records during (c) Nectalis-1 and (d) Nectalis-2.

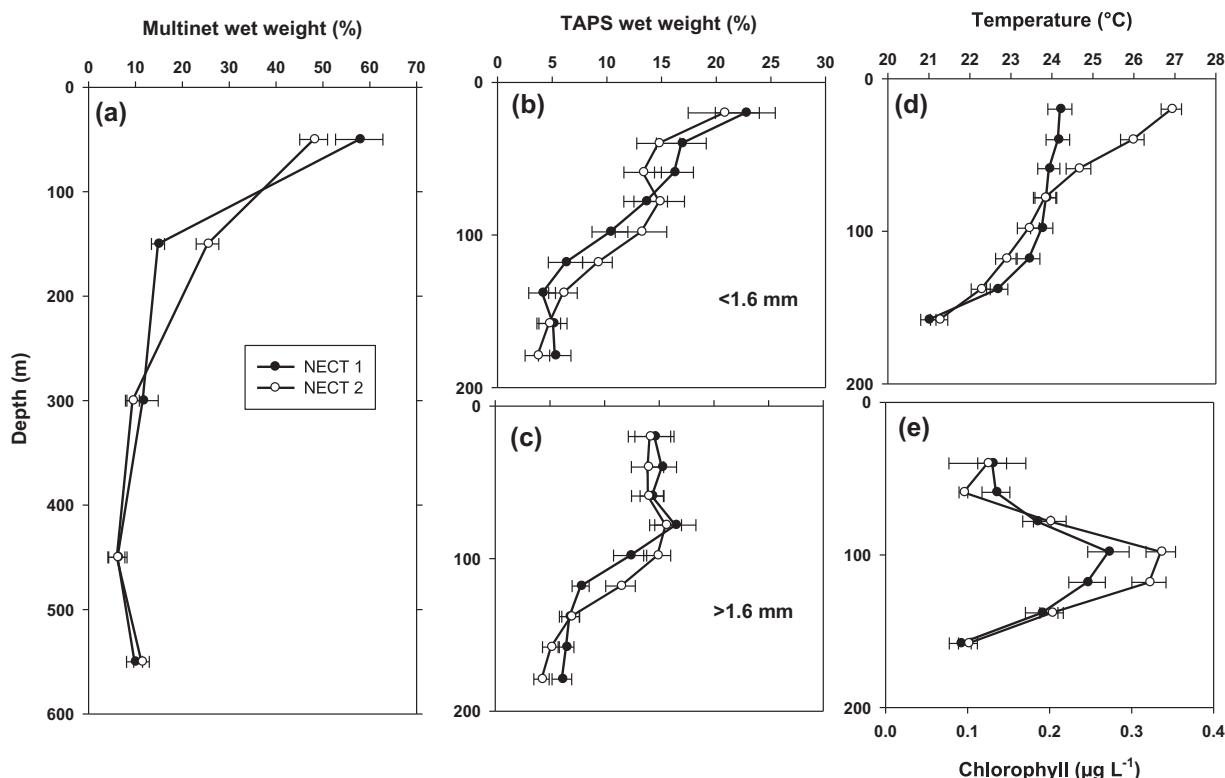


Figure 8. Mean vertical profile of (a) zooplankton wet weight from Multinet and zooplankton wet weight from TAPS for the (b) small (ESR<1.6 mm) and (c) large (ESR>1.6 mm) organisms. Wet weight at each depth is presented as a percentage of the total integrated biomass. (d) Temperature and (e) chlorophyll-a concentration profiles from CTD. Filled and open circles are Nectalis-1 and Nectalis-2 data points, respectively.

recorded by the TAPS: (1) below the surface (~20 m) and (2) slightly above the DCM (at ~80 m depth on average). The surface peak was probably slightly underestimated, due to the 6 m exclusion zone of the TAPS. This peak was mostly made up by mesozooplankton (ESR<1.6 mm; Figure 8b), while large mesozooplankton / macrozooplankton (ESR>1.6 mm) prevailed above the DCM (Figure 8c). Both of these size classes showed slightly higher biomass above the DCM during Nectalis-1 than Nectalis-2. Below the DCM (~100–160 m) Nectalis-2 biomass was slightly higher than in Nectalis-1. However, none of the difference was significant (*U* test; $p>0.05$). Multinet data showed slightly higher mean wet weight in the first 100 m during Nectalis-1 than Nectalis-2, but the difference was not significant (*U* test; $p>0.05$). In the 100–200 m layer wet weight were higher during Nectalis-2 (*U* test; $p=0.001$).

3.3.2.2. Horizontal and Temporal Distribution

All zooplankton biomass and abundance estimators were significantly higher during night time than during day time for all considered estimators (*U* test or ANOVA, $p<0.05$; Table 3). For example, mean DW values were 1.9 mg m^{-3} for day and 4.7 mg m^{-3} for night samples during the cool season cruise. During the hot season cruise, mean DW was 1.24 mg m^{-3} for day and 2.24 mg m^{-3} for night samples (Figure 1).

DW was significantly higher during Nectalis-1 than during Nectalis-2 (Table 3). Mean zooplankton abundance was also higher during Nectalis-1, but the difference was not significant ($p=0.051$). We found no significant difference between the two cruises or between day and night for the percentage of the main zooplankton groups (Table 3).

Zooplankton abundance and DW were higher north of the survey area during Nectalis-1 (stations 8–14, Figures 9a and 9c) while no clear pattern was observed during Nectalis-2 (Figures 9b and 9d). The highest abundances were measured in the vicinity of the thermal front region during Nectalis-1 at stations 12 and 13 (maximum abundance at station 13, a day-time station).

During Nectalis-1 the periphery of a cyclonic eddy was sampled at station 6 (night-time) where the highest zooplankton biovolume from TAPS for either cruise was recorded (Figure 9e) with a total 0–100 m

Table 3. Mean Values of 0–100 m Day and Night Zooplankton Abundance and Biomass Estimators Presented as the Mean ± Standard Deviation^a

Units	Mean Values ± Standard Deviation				p Values for 2 Ways-ANOVA or U Test (italicized)			
	Nectalis 1 (Cool Season)		Nectalis 2 (Hot Season)		Season	Day-Night		
	Day	Night	Day	Night	(1)	(2)	(1) X (2)	
Bv total	mm ⁻³ m ⁻³	118 ± 31.6	218.1 ± 57.6	114 ± 28.2	156 ± 23.1	0.004	0.000	0.011
Bv <1.6 mm	mm ⁻³ m ⁻³	42.59 ± 23.4	63.9 ± 32.8	37.0 ± 17.2	46.2 ± 16.36	0.114	0.018	0.463
Bv >1.6 mm	mm ⁻³ m ⁻³	75.48 ± 22.8	154.1 ± 27.0	77.2 ± 13.5	109.4 ± 22.15	0.051	0.000	0.012
B _{ADCP} ^b	mg m ⁻³	0.9 ± 0.4	10.4 ± 7.3	0.9 ± 0.5	6.4 ± 3.2	<i>0.476</i>	0.000	
Dry weight	mg m ⁻³	1.9 ± 1.3	4.7 ± 2.2	1.7 ± 0.8	2.4 ± 0.8	0.004	0.000	0.019
Wet weight	mg m ⁻³	14.4 ± 11.7	27.7 ± 15.4	13.2 ± 8.1	17.4 ± 4.6	0.098	0.014	0.184
BIO ZooScan	mg m ⁻³	7.9 ± 3.2	14.8 ± 11.3	7.4 ± 2.6	14.2 ± 6.7	0.812	0.002	0.986
Total ABD Multinet	ind m ⁻³	182 ± 119.8	359.9 ± 161.8	174 ± 53.3	235 ± 52.4	0.051	0.001	0.087
% Calanoids		41.7 ± 6.1	43.3 ± 3.6	37.4 ± 7.3	43.3 ± 7.4	0.409	0.887	0.764
% cyclopids		32.1 ± 5.5	28.9 ± 3.5	29.4 ± 7.1	31.6 ± 4.5	<i>0.337</i>	<i>0.337</i>	
% harpacticoids		0.7 ± 1.2	0.1 ± 0.1	0.6 ± 0.8	0.3 ± 0.5	<i>0.749</i>	<i>0.110</i>	
% other crustaceans		3.3 ± 1.3	5.3 ± 2.5	3.2 ± 1.2	3.3 ± 1	0.183	0.307	0.976
% gelatinous		11.5 ± 3.9	14.4 ± 6.2	15.4 ± 10.5	10.8 ± 5	<i>0.749</i>	<i>0.337</i>	
% molluscs		0.9 ± 0.8	1.7 ± 1.6	1.8 ± 1	1.3 ± 1	0.282	0.981	0.684
% protozoans		9.2 ± 3.9	6.7 ± 3.8	11.6 ± 4.7	8.5 ± 3	0.045	0.125	0.541
% meroplankton		0.7 ± 0.6	0.8 ± 0.2	0.7 ± 0.2	0.9 ± 0.4	0.585	0.521	0.67
Diversity (Shannon)	bit ind ⁻¹	4 ± 0.2	4.2 ± 0.1	4.1 ± 0.3	4.1 ± 0.3	0.811	0.908	0.693

^aThe p value of two-way ANOVA or Mann-Whitney (U test) are presented testing for season (1) and day/night (2) effects and their interactions (1X2, only in the case of ANOVA). Bold numbers refer to significant p values. U tests were performed when the transformed data were not normally distributed.

^bBiomass from ADCP was derived from the 16–104 m backscatter data. Abbreviations: Bv= biovolume; BIO= biomass; ABD= abundance; ind= individual.

zooplankton biovolume (Bv) of 326 mm³ m⁻³ (mean Nectalis-1 night Bv=218 mm³ m⁻³). In addition to the presence of this cyclonic eddy, this exceptionally higher biovolume was measured after a period of strong wind forcing (from 2 to 6 August) with wind speed reaching up to 38 knots. At station 10, the periphery of a major mesoscale cyclonic eddy was sampled (diameter of ~400 km, Figure 4) and had the highest DW for both cruises with a value of 7.36 mg m⁻³ (Figure 9c). This station was distinct by the high abundance of the molluscs group (10 ind m⁻³ at station 10, mean cruise value = 2.5 ind m⁻³).

During Nectalis-2 two major mesoscale anticyclonic eddies (diameters of ~300 km) were sampled at stations 7 and 9 (Figure 4). Station 7 was located in the frontal zone of the first eddy and station 9 in the central part of the second (Figure 4). At station 7, a day-time station, the highest 0–100 m WW during Nectalis-2 was measured with a value of 35 mg m⁻³ (Figure 9d) with an increase of gelatinous zooplankton (mostly appendicularian) contribution to the total abundance (101 ind m⁻³ at station 7, mean cruise value = 29 ind m⁻³). Station 9 had a low value of DW and WW (Figure 9d), although a night time station. The biovolumes from the TAPS were low for both stations 7 and 9.

3.3.3. Continuous ADCP and EK60 Data Records

For both cruises the continuous ADCP data recorded along the ship tracks showed higher biomass from sunset to dawn every day in the 16–104 m depth range (Figure 10). The same pattern was observed in the EK60 backscatter data (Figures 7c and 7d). U test performed on the ensemble of the two cruises showed that the B_{ADCP} was significantly higher (p<<0.001) at night (mean value of 9.72 ± 0.11 mg m⁻³, n=4299) than during the day (mean value of 2.12 ± 0.04 mg m⁻³, n=4275). The continuous estimates of B_{ADCP} showed a weakening of the diel signal in relation to higher SST during both seasons. During both cruises, higher B_{ADCP} (night-time) was associated with lower SST in the south of the survey area. This trend is confirmed by negative rank-correlations between night B_{ADCP} and SST (Rs=−0.25, p<<0.001) for Nectalis-1 and Rs=−0.23, p<<0.001 for Nectalis-2). The same trend was observed in the EK60 backscatter data which also showed negative rank-correlations with SST (Rs=−0.32, p<<0.001 for Nectalis-1 and Rs=−0.24, p<<0.001 for Nectalis-2). Cross-correlation and coherence analyses showed no significant phase lag between the B_{ADCP} (or EK60 backscatter) and the SST.

Nonparametric rank correlation analysis performed on continuous data recorded along the ship tracks (ensemble of the two cruises) showed that the night-time B_{ADCP} and EK60 backscatter were significantly related to latitude (Rs=−0.42 and −0.43, respectively, p<<0.001) and FSLE (proxy for the presence of

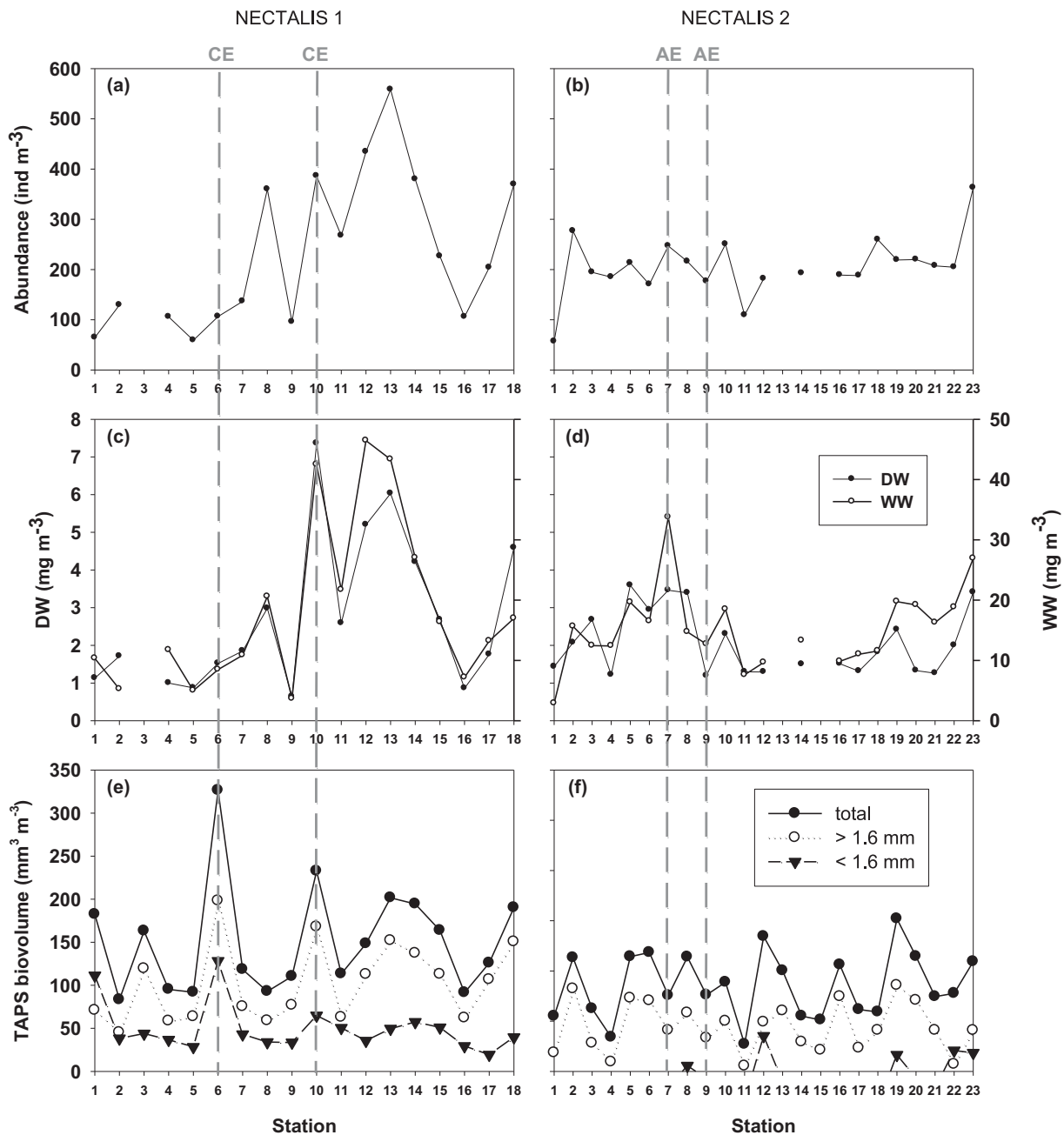


Figure 9. Depth-integrated (0–100 m): (a and b) zooplankton total abundance, zooplankton (c) dry weight (DW, filled circle) and (d) wet weight (WW, open circle), and TAPS total (filled circles), (e) >1.6 mm (open circles) and (f) <1.6 mm (triangles) biovolume. Gray dashed lines show the stations where eddy features were present: cyclonic eddy (CE) and anticyclonic eddy (AE). Nectalis-1 data are presented on the left column and Nectalis-2 on the right column.

fronts, $R_s=0.31$ and 0.26 , respectively, $p < < 0.001$). The latitude was correlated to SSS ($R_s=0.61$, $p < < 0.001$) and SST ($R_s=0.29$, $p < < 0.001$).

3.3.4. Zooplankton Community

A detailed description of zooplankton taxa down to the species level is presented in Table 4. A total of 117 zooplankton taxa were recorded during Nectalis cruises including 66 copepod and 51 noncopepod taxa (other crustaceans, gelatinous organisms, molluscs and meroplanktonic larvae). A slightly higher number of taxa was recorded during Nectalis-2 (109) than during Nectalis-1 (92), although the diversity index was similar during both cruises with a Shannon diversity index of $4.06 \pm 0.04 \text{ bit ind}^{-1}$ for Nectalis-1 and 4.04 ± 0.06

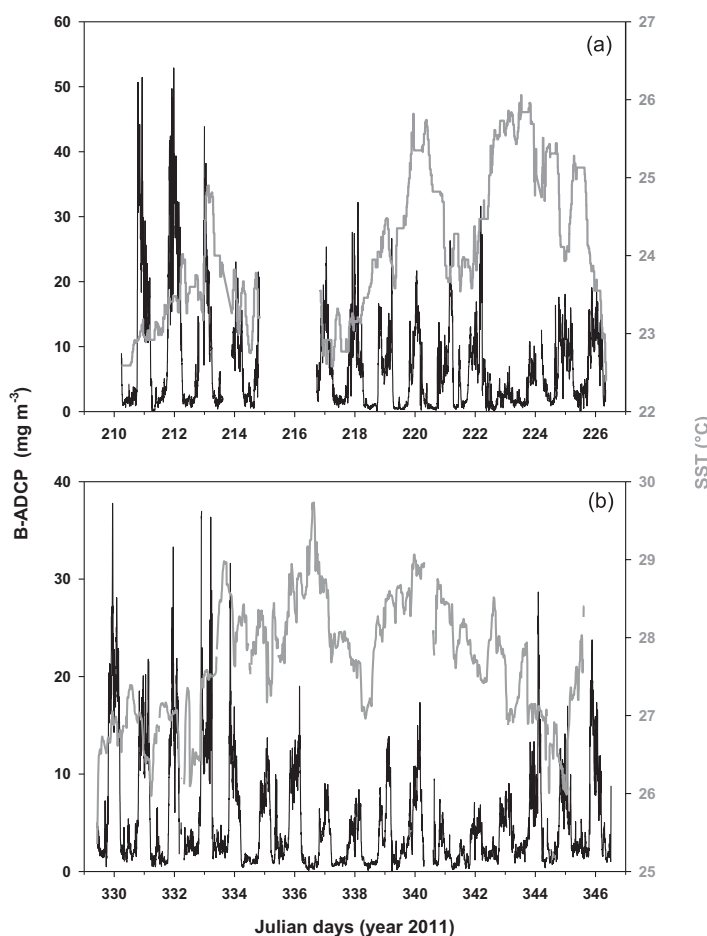


Figure 10. Depth integrated (16–104 m) zooplankton biomass (black lines) estimated from ADCP (B_{ADCP}) and sea surface temperature (SST - gray lines) during (a) Nectalis-1 and (b) Nectalis-2.

bit ind^{-1} for Nectalis-2. Copepods were highly dominant, representing 73.2 and 71.5% of the total abundance during Nectalis-1 and Nectalis-2 respectively. Among copepods, calanoids prevailed (40–42% of total abundance), with *Paracalanus* spp. (16–17%), *Clausocalanus* spp. (3–6%), *Acartia* spp. (2–5%) and *Mecynocera clausi* (2–5%) as the dominant species. Cyclopoids (30–31% of total abundance) were mostly represented by *Oncaea* spp. (8–11%), *Corycaeus* spp. (8–8.5%) and *Oithona* spp. (8–10%). Harpacticoids contribution was low (0.4–0.5% of total abundance) with *Macrosetella gracilis* (0.4%) as the most represented species. Gelatinous organisms (mainly appendicularians and chaetognaths) accounted for 12–13% of the abundance, while other crustaceans (mainly ostracods and euphausiids) represented 3–4%.

The NMDS ordination of the zooplankton taxa abundance data (stress value of 0.14 indicating a strong ordination)

identified four clusters (Figure 11a), two in Nectalis-1 (Clusters 1 and 2) and two in Nectalis-2 (clusters 3 and 4). The comparatively wider spread of clusters 1 and 2, and close grouping of Clusters 3 and 4 indicated that species composition was overall more similar during Nectalis-2 than Nectalis-1.

The spatial distribution of zooplankton station clusters showed a similar pattern for both cruises, with stations to the south and west of the study area (stations 1–9 for Nectalis-1 and stations 2–15 for Nectalis-2) separating from stations to the east and north of the study area (stations 10–18 for Nectalis-1 and stations 16–23 for Nectalis-2) (Figures 11b and 11c). Multiple regression analysis showed that the environmental variables that were most strongly linked to the species abundance distribution (represented by the first two dimensions of the NMDS) were salinity ($R^2=0.265$, $p=0.006$) and latitude ($R^2=0.201$, $p=0.03$), both variable being highly correlated ($R^2=0.61$; $p=0.0001$).

Overall, within cluster similarity between stations was high (> 70%) while dissimilarity between cluster ranged between 41% for clusters 1 and 2, and 24% for clusters 3 and 4, indicating a greater spatial variability in zooplankton community composition (primarily along a north-south axis) during Nectalis-1 than Nectalis-2. Most of the dissimilarity between clusters was due to variation in the abundance of the same pool of species, and there were few species unique to a single cluster. During Nectalis-1, the higher abundance and biomass of zooplankton in the northeastern part of the survey area compared to the southwest may explain the relatively high dissimilarity between clusters 1 and 2.

Zooplankton taxonomic composition showed differences between the colder SW waters (Clusters 1 and 3) and the warmer NE waters (clusters 2 and 4). Largest organisms (size >5 mm, including Chaetognaths, siphonophores, eupausiids and decapod larvae) had higher percentage of abundance in clusters 1–3 than

Table 4. Mean Values of 0–100 m Abundance (ind m⁻³) and Estimated Length (mm) of the Zooplankton Taxa in the Four Clusters Defined in the NDMS Analysis: Clusters 1 and 2 (CI 1, CI 2) for Nectalis-1 and Clusters 3 and 4 (CI 3, CI 4) for Nectalis-2^a

Taxa	Length ^b	Nectalis-1				Nectalis-2				
		CI 1	CI 2	CI 3	CI 4	CI 1	CI 2	CI 3	CI 4	
COPEPODS		84.4	266.9	155.7	188.8	OTHER CRUSTACEANS	4.2	15.8	8.4	8.5
Copepod nauplii	0.5		0.60	1.27	0.30	AMPHIPODA				
CALANOIDA						<i>Hyperia</i> sp.			0.16	0.16
<i>Acartia</i> spp.	1	2.26	9.29	9.74	11.23	<i>Oxycephalidae</i>		0.13	0.06	
<i>Acrocalanus monachus</i>	1		1.64	0.35	0.31	<i>Phronima sedentaria</i>	0.04	0.24	0.12	0.09
<i>Acrocalanus</i> spp.	1			0.44	0.24	<i>Platyscelus</i> sp.			0.06	
<i>Aetideus giesbrechti</i>	1.7	0.12	0.23	0.11	0.12	<i>Primno</i> sp.			0.17	0.12
<i>Calanus</i> spp.	2	2.38	6.47	6.31	8.71	<i>Pronoe</i> sp.			0.13	
<i>Calanopia minor</i>	1.2	0.02	1.97	1.02	0.14	<i>Scina</i> sp.		0.19		
<i>Calocalanus pavo</i>	0.8	0.96	2.86	1.47	0.89	<i>Streetsia</i> sp.				0.07
<i>Calocalanus plumulosus</i>	0.8	0.91	2.54	1.23	0.58	<i>Themisto</i> sp.	0.13	0.26		
<i>Calocalanus tenuis</i>	1.1	0.58	2.61	2.02	1.12	<i>Vibilia</i> sp.			0.08	0.07
<i>Calocalanus</i> sp.	1	1.03	1.79	0.82	1.04	CLADOCERA				
<i>Candacia</i> spp.	1.7	1.29	2.98	0.67	0.38	<i>Evadne</i> sp.			0.09	2.20
<i>Canthocalanus</i> spp.	1.5	1.74	2.37			<i>Podon</i> sp.				0.06
<i>Centropages violaceus</i>	1.8	1.24	3.14	0.24	0.11	EUPHAUSIDS	0.55	4.98	2.72	2.04
<i>Centropages</i> spp.	1.8			0.06	0.06	ISOPODS	0.08	0.21	0.21	0.06
<i>Chirundina</i> ou <i>Euchirella</i>	2.5		0.19			LEUCIFERS	0.04	0.14	0.23	0.14
<i>Clausocalanus furcutus</i>	1.2	5.32	23.14	4.97	9.59	MYSIDS	0.13	0.23	0.21	0.20
<i>Paracalanus</i> spp.	0.9	15.33	65.56	24.96	51.10	OSTRACODS	3.27	9.44	4.12	3.28
<i>Cosmocalanus darwini</i>	2		0.42	0.96	0.28					
<i>Euaugaptilus hecticus</i>	2.5			0.04		GELATINOUS	10.1	56.3	30.3	21.3
<i>Euchaeta</i> spp.	3.5	3.00	6.57	1.59	0.78	Chaetognaths	2.49	6.45	9.27	7.23
<i>Euchirella</i>	4		0.06	0.07	0.17	Appendicularians	5.90	42.23	18.43	11.73
<i>Gaetanus pileatus</i>	5		0.06	0.06	0.07	Doliolids	0.20	1.62	0.44	0.20
<i>Haloptilus acutifrons</i>	3			0.13		Jellyfishes	0.59	1.40	0.65	0.26
<i>Haloptilus longicornis</i>	2			0.37	0.24	Pyrosoma		0.06		
<i>Haloptilus</i> spp.	2.5	0.18	1.08	0.43	0.07	Salps	0.22	1.60	0.13	0.21
<i>Heterorabdus</i> sp.	2	0.30	0.20	0.34	0.30	Siphonophores	0.74	2.94	1.37	1.62
<i>Lucicutia clause</i>	1.8			0.04						
<i>Lucicutia flavicornis</i>	1.8	1.14	8.15	2.74	6.54	MOLLUSCS	2.0	4.2	4.5	1.8
<i>Lucicutia ovalis</i>	1.5	0.15	0.11	0.21	0.47	<i>Cavolinia</i>	0.17	0.20	0.52	0.21
<i>Lucicutia</i> sp.	1.7			0.04	0.54	<i>Creseis</i>	0.55	0.27	0.45	0.17
<i>Mecynocera clausi</i>	1	4.15	1.70	11.95	7.41	<i>Limacina</i>	1.00	2.84	3.07	0.86
<i>Nannocalanus minor</i>	1.5	2.12	3.66	0.54	0.73	GYMNOSOMA				0.08
<i>Par/Sub/Eucalanus</i> spp.	4.5	0.38	1.55	0.13	0.54	HETEROPODA				
<i>Pareucalanus attenuatus</i>	4.5			1.63	0.21	<i>Atlanta</i> spp.		0.06	0.04	0.06
<i>Phaenna</i> sp.	2	0.07	0.13	0.05	0.09	Pterotrachea spp.		0.23		0.10
<i>Pleuromamma abdominalis</i>	3	1.91	8.17	0.60	0.52	POLYCHAETS	0.22	0.57	0.44	0.29
<i>Pleuromamma</i> sp.	3	0.35	0.45	2.41	8.07					
<i>Pleuromamma xiphias</i>	4			0.08		PROTOZOA	7.4	34.7	20.6	21.0
<i>Pontellina plumata</i>	1.5	0.06	0.10	0.06	0.13	Foraminifera		4.30	1.74	0.67
<i>Rhincalanus rostrifrons</i>	2.7		0.07	0.17		<i>Noctiluca</i> sp.	6.39	27.49	17.94	19.64
<i>Rhincalanus</i> sp.	3		1.77			Radiolarians	1.03	2.66	0.90	0.65
<i>Scaphocalanus</i> spp.	2.5	0.14		0.08	0.20	Tintinnids		0.24		
<i>Scolecithricella</i> spp.	1.5	0.38	2.34	0.21	0.50					
<i>Scolecithricella tenuiserrata</i>	1.2	0.47	0.24			MEROPLANKTON	1.4	5.2	2.1	2.5
<i>Scolecithrix bradyi</i>	1.2	0.28	1.68	0.09	0.21	Branchiostoma			0.10	
<i>Scolecithrix danae</i>	1.8	0.29	0.93	0.83	0.40	Cephalopod larvae	0.06			
<i>Scolecithrix</i> spp.	1.5		0.15			Cirriped larvae	0.30		0.26	0.19
<i>Subeucalanus subtenuis</i>	2.8			1.67		Cyphonaute larvae	0.5		0.04	0.27
<i>Temora discaudata</i>	1.8		0.06		0.72	Decapods larvae	0.33	1.36	0.50	0.32
<i>Temora stylifera</i>	1.5	0.04	0.16	0.22	0.24	Echinoderm larvae		2.31	0.05	
<i>Tortanus gracilis</i>	1.6	0.38	1.14			Fish eggs	0.41	0.52	0.38	0.34
CYCLOPOIDA						Fish larvae	0.05	0.17	0.31	0.33
<i>Copilia</i> spp.	4	0.38	0.24	0.45	0.20	Gastropod larvae				0.06
<i>Corycaeus</i> spp.	1	8.15	26.07	17.94	20.90	Lamellibranch larvae	0.11	0.42	0.12	0.11
<i>Lubbockia</i> sp.	2		0.21	0.20	0.20	octopus larvae				0.09
<i>Oithona plumifera</i>	0.7	7.24	7.63	2.80	0.93	Phyllosoma larvae				0.06
<i>Oithona robusta</i>	1.2			2.51		Polychaets larvae	0.10	0.42	0.10	0.14
<i>Oithona tenuis</i>	1			4.20	3.65	Sepia larvae				0.07
<i>Oithona</i> spp.	1	8.60	20.98	26.06	23.62	unidentified larvae	0.06		0.29	0.52
<i>Oncaea</i> spp.	0.8	9.91	42.26	17.16	22.19					
<i>Saphirina</i> spp.	2	0.25	0.29	0.21	0.17					
HARPACTICOIDA										

Table 4. (continued)

Taxa	Length ^b	Nectalis-1				Nectalis-2			
		Cl 1	Cl 2	Cl 3	Cl 4	Cl 1	Cl 2	Cl 3	Cl 4
<i>Aegisthus magnus</i>	1.8				0.07				
<i>Clytemnestra</i> spp.	1	0.11	0.21	0.08	0.10				
<i>Macrosetella gracilis</i>	1.2	0.55	0.61	0.57	1.34				
<i>Microsetella</i> sp.	0.8	0.24	0.10	0.04	0.07				

^aSee Figure 10 for the clusters distribution.

^bApproximative size according to Razouls et al. [2011–2014] and Trégouboff and Rose [1957].

in clusters 2–4, while small copepods (*Oncaea*, *Corycaeus*, *Paracalanus* and *Clausocalanus*) prevailed in clusters 2–4 (Table 4; U test, $p < 0.05$). Another important difference is the higher abundance of the copepod *Mecynocera clausi* in clusters 1–3 (U test, $p < 0.05$). This trend was confirmed with the size-distribution derived from the ZooScan analyses, with significantly ($p < 0.05$) lower mean size values in cluster 2 ($670 \pm 13 \mu\text{m}$) compared to cluster 1 ($712 \pm 23 \mu\text{m}$) and in cluster 4 ($623 \pm 12 \mu\text{m}$) compared to cluster 3 ($646 \pm 25 \mu\text{m}$).

4. Discussion

4.1. Method Comparison

Significant correlations between the different estimators at sampling stations showed relatively good agreement between methods to estimate zooplankton biomass. Wet biomass estimated with the ZooScan showed slightly lower values than the Multinet wet weight measurements. This difference may be due to the removal of detritus in the image processing tool [Picheral, 2011]. The low correlations of the TAPS biovolume < 1.6 mm with the Multinet estimators (not significant with the ZooScan estimators) may have been induced by a higher sensitivity of the TAPS to smaller particles. As observed above, in the results section, the one order on magnitude difference between the wet biomass from the TAPS and the Multinet is at odds with previous comparisons in other regions [e.g., Lebourges-Dhaussy et al., 2009, 2014] and at present we do not have a clear explanation for this discrepancy [Menkes et al., 2014]. A possible explanation could be linked to the wider size range (0.05–3 mm) sampled by the TAPS compared to the Multinet (0.2 to few mm). Net avoidance may also be a hypothesis to explain the discrepancy between TAPS and Multinet biomass estimates, as it has been demonstrated by Wiebe et al. [2013] for euphausiids and by Fleminger and Clutter [1965] for copepods. The size range to be considered to compare the results should thus be limited to what is expected to be a common range. Significant correlations were also observed between ADCP backscatter and TAPS, with higher correlation when considering the larger TAPS fraction than the smaller one. The TAPS is probably more representative of micro and mesozooplankton and less of the larger part of the organisms than the Multinet in situation of oblique tows at a sufficient speed to limit avoidance as in Lebourges-Dhaussy et al. [2014]. But in the present work, the tows were vertical in fixed position, so the largest organisms seem to be better represented by the TAPS than by the multinet in this case. The ADCP is also more representative of large mesozooplankton and macrozooplankton. Hence, in our study, ADCP is likely to represent predators (macrozooplankton) and the smaller part of the TAPS detections is likely to express preys (micro and mesozooplankton).

Shipborne ADCP, provide backscatter data for many databases. Unlike biological sampling at stations, they give continuous information along the routes of ships about the distributions of zooplankton in the water column as well as vertically, although it is limited to the 16–150 m layer for an ADCP at 153 kHz such as the one used in this study. It is worth noting that shipborne ADCP backscatter measurements inherently underestimate surface zooplankton biomass due to missing the first ~ 15 m of the water column, where the backscatter is contaminated by air bubbles [Jiang et al., 2007]. In this study the correlation between the Sv and the Multinet DW, which is the standard measurement of metazooplankton biomass classically used in the literature [Harris et al., 2000], was not very high ($r = 0.51$). This low correlation may be also linked to the ADCP missing the organisms in the first 15 m of the water column. Although the r value is low, the relationship between zooplankton DW and ADCP backscatter intensity is highly significant ($p < 0.001$). Further, the purpose of this study is to examine variability in zooplankton as related to environmental conditions rather than establishing quantitative estimates of zooplankton populations. Other studies, using the same type of

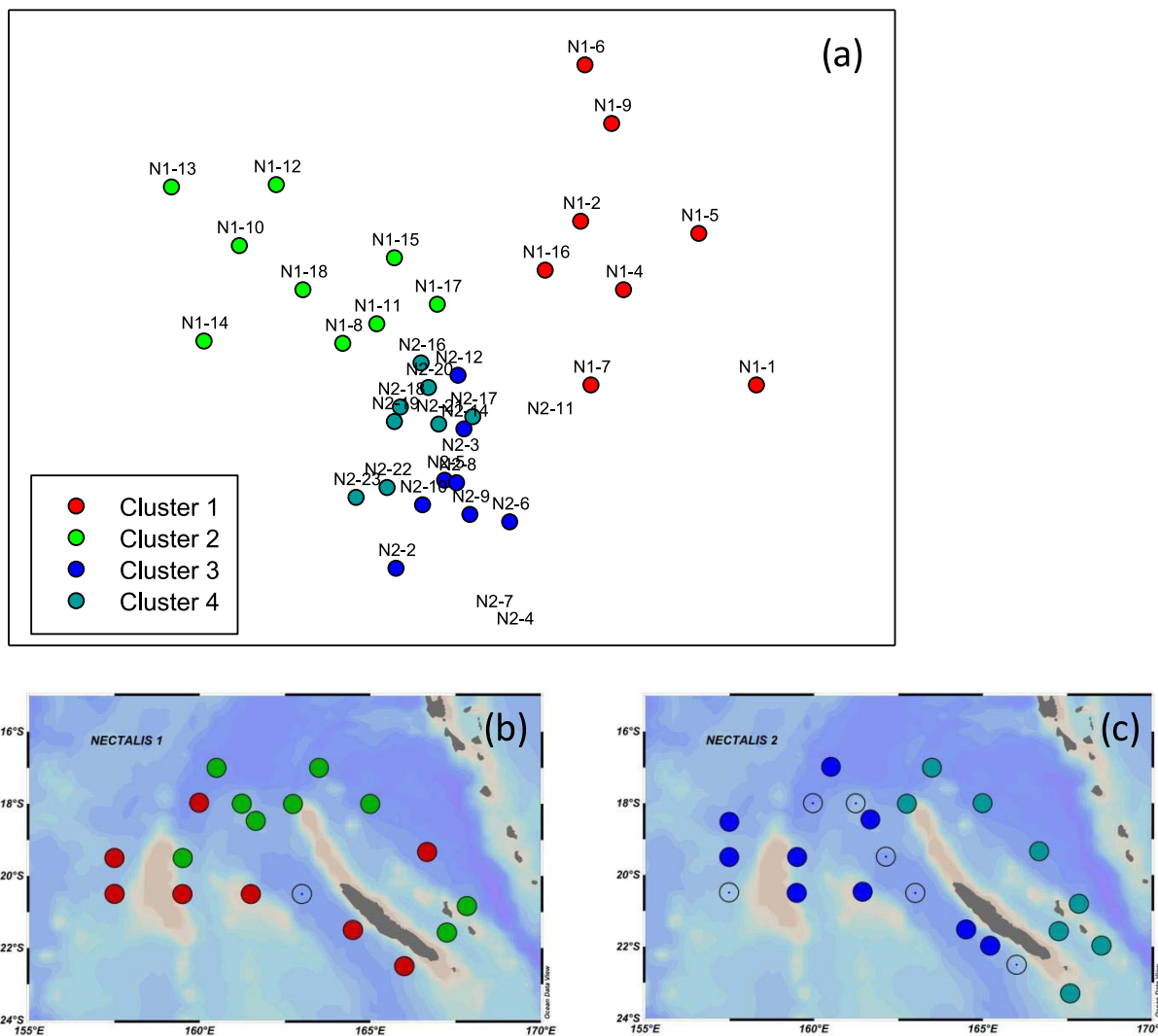


Figure 11. Nonmetric Multi-Dimensional Scaling (NMDS). (a) Ordination of the zooplankton taxa abundance (square root transformed data). The axes (unitless) are the first two dimensions of the ordination (2-D ordination) and express stations relationship in ordination space. NMDS clusters spatial distribution during (b) Nectalis-1 and (c) Nectalis-2. The open circle symbol in Figure 11b represents station where no zooplankton abundance data were available (station 3) and in Figure 11c represent outliers in the cluster analysis except stations 13 and 15 where no zooplankton abundance data were available.

ADCP, found similar results for the backscatter-net biomass calibration. *Jiang et al.* [2007], in the Sargasso Sea off Bermuda, found calibration results ($R = 0.50$, $p < 0.05$ for 165 data points) similar to those we report ($R = 0.51$, $p < 0.05$ for 38 data points). *Heywood et al.* [1991] off the island of Albadra in the Indian Ocean, found a correlation coefficient of 0.57 significant at $p < 0.05$ for 62 data points, fitting an exponential regression curve to their ADCP backscatter-zooplankton biomass relationship.

Large organisms (e.g., large copepods, euphausiids, salps, chaetognaths), relatively abundant in our samples, especially at night, may explain the difference between Multinet and ADCP biomass estimates through net avoidance by these large organisms [Zhou et al., 1994; Wiebe et al., 2013]. The avoidance becomes more important for nets with small mouth area [Harris et al., 2000] (0.25 m^2 in our study) and for fixed vertical tows, highlighting the interest of using non invasive and continuous samplers such as the ADCP for biomass estimates. At higher abundance (night time sampling) zooplankton biomass from Multinet in our study was underestimated by ~ 2 order of magnitude compared to the ADCP-derived biomass. This is also the ratio obtained with the biomass estimated from the TAPS for the $> 1.6 \text{ mm}$ ESR size range. Similar results were found by Zhou et al. [1994] near the Antarctic Peninsula.

A long record of studies has demonstrated the effectiveness of ADCP backscatter for documenting patterns in zooplankton biomass and estimates of the patchiness [e.g., *Ashjian et al.*, 1994, 2002; *Batchelder et al.*, 1995; *Jiang et al.*, 2007]. It has been shown that the major part of the backscatter signal from RDI's 153 kHz ADCP is mostly representative of macrozooplankton, as demonstrated by *Burd and Thomson* [2012] who determined that ADCP volume backscatter accounted for 84% of the variance of zooplankton biomass from net tows. In our study, ADCP backscatter showed a better correlation with the biomass of the larger zooplankton fraction (>1.6 mm) than the smaller fraction (<1.6 mm), from ZooScan and TAPS (Table 2), confirming the relevance of using ADCP for large organisms (macrozooplankton, and, to a certain extent, micronekton). Recently, *Menkes et al.* [2014], in their comprehensive paper describing the Nectalis program results (from physics to micronekton), suggested that the 153 KHz ADCP backscatter data (Sv) probably also include information on the micronekton (2–20 mm) abundance, as they found significant correlation between the backscatters from the ADCP and a calibrated multifrequency scientific echo sounder that detects zooplankton, micronekton and larger organisms.

4.2. Zooplankton Variability in the EEZ

4.2.1. Vertical and Diel Variability

During both seasons, the average vertical distribution of TAPS biomass estimates showed that smaller organisms (<1.6 mm) were more abundant in the upper 50 m while larger organisms (>1.6 mm) were more evenly distributed in the upper 100 m with maximum values near the DCM. The vertical distribution of zooplankton in the South West Pacific is poorly documented. Higher concentration of zooplankton in surface water, as observed in this study for meso size classes, salps and chaetognaths, appears to be common in the HNLC (High Nutrient low Chlorophyll) zone of the equatorial upwelling zone (5°S–5°N) [*Roman et al.*, 2002], but to our knowledge it was never described in the LNLC (Low Nutrient low Chlorophyll) zone off New Caledonia. Off the coast of East Australia, *Young et al.* [2011] reported enhanced concentrations of zooplankton in surface waters to be mostly related to macrozooplankton, mainly gelatinous organisms (chaetognaths and salps), as also found in this study. The uniform distribution of large zooplankton in the first ~100 m in this study is consistent with the general vertical distribution pattern of zooplankton in oligotrophic regions North and South of the equator and in the Warm Pool in the western equatorial Pacific [*Roman et al.*, 2002].

Association of high biomasses of zooplankton with DCM as seen in this study (for the larger TAPS fraction), to our knowledge, has not been demonstrated in the tropical pacific region.

The maximum of biomass or abundance of zooplankton was observed at the same depth or in the vicinity of the depth of the DCM during a cross-Mediterranean cruise [*Nowaczyk et al.*, 2011] for nauplii and copepods, in California ([*Pieper and Holliday*, 1984] for copepods) and in the Mozambique Channel [*Lebourges-Dhaussy et al.*, 2014] for ESR: 0.2–0.5 and 1–3 mm size classes in cyclonic features).

In addition to size related structuring of the zooplankton distribution in the water column related to the DCM, a clear diel pattern was observed in the zooplankton vertical distribution as demonstrated by the ADCP signal and by higher values of zooplankton biomass observed at night by all sampling techniques. Previous zooplankton studies based on acoustic backscatter from the RDI 153 kHz ADCP, have reported this diel cycle of zooplankton biomass/abundance in the equatorial Pacific [*Radenac et al.*, 2010], the northwestern Atlantic [*Jiang et al.*, 2007; *Smeti et al.*, 2010] and the northern Indian Ocean [*Ashjian et al.*, 2002]. This diurnal cycle is typical of most of the world's oceans with vertically migrating organisms swimming toward the surface during night time (at sun set) and into deeper waters during day-time (at dawn). This diel vertical migration (DVM) signal has been found in previous studies in coastal waters of New Caledonia islands [*Le Borgne et al.*, 1997] but has not been demonstrated in the deep Coral Sea off New Caledonia.

4.2.2. Horizontal Variability

4.2.2.1. Mesoscale Events

In this study, mesoscale eddies appeared to be associated with substantial increased zooplankton biomass in surface waters such as at the periphery of an anticyclonic eddy during Nectalis-2 (station 7). The mechanism by which eddy dynamics act on zooplankton biomass is complex, and a variety of eddy-related process could explain higher zooplankton biomass associated with these features, e.g., eddy pumping (cold core eddies) that leads to injection of nutrients in the euphotic layer promoting the production cascade

[McGillicuddy *et al.*, 1998; McNeil *et al.*, 1999]. Enhanced primary production has also been observed during both cruises mainly at the center of several cyclonic eddies [Menkes *et al.*, 2014].

Also frontal aggregation of zooplankton biomass can occur at anticyclonic eddies peripheries [e.g., Labat *et al.*, 2009; Yebra *et al.*, 2009; Smeti *et al.*, 2010; Cotté *et al.*, 2011], where cells of vertical velocities create localized upwelling that inject nutrients into the surface layer [Lévy, 2008]. Growth rates have been reported to be enhanced at the edge of anticyclonic eddies [Hernandez-Leon *et al.*, 2001]. In the regions encircling these features, elevation of the pycnocline and in most cases, of the nutricline, can boost primary and secondary production [Longhurst, 2007]. Conversely, the center of anticyclonic eddies is a region of isopycnal depression, causing water to sink leading to decreased plankton biomass in surface waters. Accordingly, station 9 of Nectalis-2 sampled the core of an anticyclonic eddy and was associated with low zooplankton biomass, despite sampling occurring at night when we expect higher surface zooplankton biomass. Frontal aggregations were observed in the northern part of our study region where a tight thermal front was established during the cool season (Nectalis-1), where higher biomass and abundance were observed at stations 12 and 13 (although day-time stations) located in the frontal region. In addition to this mesoscale scale thermal front north of the EEZ, we found statistically significant association between continuous zooplankton biomass proxies (ADCP and EK60) and filaments (FSLE) suggesting a role of submesoscale fronts, in addition to mesoscale eddies and fronts, in structuring zooplankton distribution in space and time [Cotté *et al.*, 2011]. Spikes of production and biomass aggregation induced by eddies and fronts can be particularly important in the oligotrophic conditions-like the interior of subtropical gyres, the shallow and nutrient-depleted photic layer occurring in summertime [Cotté *et al.*, 2011, North and South of the equator and in the Warm Pool in the western equatorial Pacific [Roman *et al.*, 2002].

The increase or decrease of zooplankton biomass associated with these oceanographic features, was not detected by all zooplankton sampling devices used in this study (Multinet, TAPS, ADCP, EK60). This could be explained by the fact that each instrument measures a different size range of zooplankton that may have responded differently to the presence of the mesoscale features (eddy and front). For example, at the cyclonic eddy sampled at station 6 during Nectalis-1, exceptionally high TAPS biovolume and low DW from the Multinet were observed. This suggests a greater contribution of smaller organisms to surface zooplankton concentration, as evidenced by the higher TAPS biovolume of small zooplankton ($ESR < 1.6$ mm) at this station (see Figure 9e). At the same location, wind-eddy interactions [see McGillicuddy *et al.*, 2007] may also have contributed to enhance zooplankton biomass through eddy pumping.

Similar observation of enhanced zooplankton biomass in relation to mesoscale eddies have been documented in various parts of the world ocean. For example, this relation has been demonstrated in the north Pacific and the northwestern Atlantic [e.g., Benitez-Nelson and McGillicuddy, 2008; Smeti *et al.*, 2010]; in the Mediterranean Sea [Nowaczyk *et al.*, 2011] and in the Mozambique Channel [Lebourges-Dhaussy *et al.*, 2014; Béhagle *et al.*, 2013].

4.2.2.2. Relationships Between Zooplankton and Water Masses

Two water masses were encountered in the studied area during Nectalis cruises [Menkes *et al.*, 2014]: (1) north of 19°S – 20°S , waters were characterized by warm temperature, low salinity, low nitrate and lower primary production, representative of the Coral Sea oligotrophic regime and largely influenced by the warmer and fresher waters of the South Pacific Convergence Zone; (2) south of 19°S – 20°S , waters under the influence of the return flow from the East Australian Current with lower temperature, higher salinity, shallower nitracline, higher nitrate content in the surface layer, higher primary production and higher surface chlorophyll. In the northern warm water mass we observed lower overall ADCP-derived zooplankton biomass and clear attenuation of the diel migration in the upper layer (0–100 m), while to the south, in the colder water mass, the opposite occurred. This pattern is in agreement with what was described in Le Borgne *et al.* [2011]. These authors interpreted the increased proportion of mesozooplankton, occurring within the first 100 m, as a result of the nitracline shoaling and the associated increased new primary production. Through its control on the distribution of primary production the depth of the nutricline also affects the absolute biomass and the diel migrations of mesozooplankton. When the nitracline is deep, enhancing oligotrophic conditions in surface waters, the vertical night-time movements of mesozooplankton are decreased. In that situation zooplankton is less likely to migrate upward as surface phytoplankton is poorly abundant. This is in agreement with the optimal foraging theory and the hypothesis that diel vertical migrations (DVM) are driven by hunger and satiation [Pearre, 2003].

In addition to the effect on the biomass our results show that the zooplankton composition was also affected by these two water masses. Indeed, the NMDS analysis performed on zooplankton taxa identified four clusters: two associated with the colder SW water mass and two associated with the warmer NE water mass. At both seasons, largest organisms (Chaetognaths, siphonophores, eupausiids and decapod larvae), had higher abundance in the cold water than in warm water, while small copepods (*Oncaea*, *Corycaeus*, *Paracalanus* and *Clausocalanus*) prevailed in cold water. This is consistent with the increased migratory biomass observed in the colder water mass and the ability of larger organisms to perform a more pronounced DVM than smaller zooplankton [Hays *et al.*, 1994]. The higher abundance of the copepod *Mecynocera clausi*, one of the most abundant calanoid reported in this study, in the cold water is consistent with its affinity for lower temperature [Paffenhöfer and Mazzocchi, 2003].

In this study, in addition to the north-south difference we also observed a seasonal difference. Unexpectedly, during the cool season (Nectalis-1), although higher net primary production was found in the south, net tow zooplankton biomass was highest in the north. It would be expected that higher primary production (NPP) would result in enhanced zooplankton biomass, and possibly increased residence time of zooplankton in the surface waters. This discrepancy may arise from the fact that we used NPP values derived from satellite surface measurements, but these values were well correlated with in situ productivity measurements [Menkes *et al.*, 2014]. During the cool season, we also observed a relatively high dissimilarity between the zooplankton community associated with the two water masses (warm-NE and cold-SW), as compared to the hot season when zooplankton community was more homogeneous.

Overall, though there do not seem to be important differences in general ecosystem properties between seasons, except for the mesoscale variability [Menkes *et al.*, 2014], our results do support the idea that mesoscale dynamics is the major factor driving spatial variation in zooplankton biomass, perhaps predominantly through biomass aggregation and advection, thus representing hotspots for consumers.

5. Conclusions

Our results bring additional evidence that the 153 KHz ADCP and the 200 KHz EK60 echosounder are valuable tools for studying zooplankton variability, particularly macrozooplankton, and provided key insights into the spatial and temporal variability of zooplankton in the New Caledonia EEZ. The use of continuously recording acoustic instruments, complemented by net sampling, provides an essential tool in studies of zooplankton variability over large spatial and temporal scales.

Our results show two important features for the distribution of the zooplankton in the EEZ:

1. Higher zooplankton biomass characterized by higher proportion of large organisms with higher DVM amplitude was associated with cold southwestern waters, while lower biomass, characterized by small zooplankton and lower DVM amplitude was associated with northeastern warm waters.
2. Substantially enhanced biomass and abundance appeared to be episodically associated with mesoscale features leading to a rather patchy distribution.

However, we cannot draw final conclusion regarding zooplankton in the New Caledonian EEZ from only two seasonal cruises that does not cover the whole EEZ (the sampling mostly covered the northern part of the EEZ). It seems that zooplankton biomass and community composition in the upper-ocean off New Caledonia is overall driven by large scale water mass circulation in the Coral Sea, with mesoscale variability introduced by eddies and fronts (which are ubiquitous features of the region). Our results points to a potentially important role of these mesoscale features as major drivers of the distribution and abundance of zooplankton and thus also as potentially important drivers for the distribution of higher trophic levels (i.e., micronekton and tuna). No comprehensive understanding of zooplankton and ecosystem dynamics in the EEZ can be achieved without taking into account the fundamentally turbulent property of the ocean. Future studies of zooplankton should give particular care when planning oceanographic cruises to investigate more specifically the impact of mesoscale (e.g., eddies, meanders and fronts) and submesoscale features on zooplankton. The sampling strategy should involve tracking several eddy features (by combining in situ measurements and satellite altimetry) and sampling of the zooplankton as well as the biogeochemistry at different locations relative to the eddies (core, periphery, and outside).

Acknowledgments

The data used in the manuscript can be requested from the NECTALIS project (<http://www.spc.int/oceanfish/en/ofpsection/ema/biological-research/nectalis>) principle investigators' Christophe Menkes (christophe.menkes@ird.fr) et Valerie Allain (valeriea@spc.int). This research was cofunded by the Institute of Research for Development (IRD), the LEFE-CYBER program, the Agence des Aires Marine Protégées (AAMP) and the New Caledonian Zone Economique de Nouvelle-Calédonie (ZoNeCo) program. H. Smeti received support from the IRD and the Tunisian Ministry of Higher Education and Scientific Research (MHESR) through their doctoral fellowship programs. We are indebted to the captain and crew of the R/V Alis for their assistance during sea operations. H. Smeti, C. Menkes and M. Pagano thank Francesco d'Ovidio for assistance with ocean filaments mapping, B. Espinasse and A. Nowaczyk for helping with the ZooScan data analysis and taxonomic sorting. The authors are indebted to two anonymous reviewers whose constructive remarks helped to improve the quality of the manuscript.

References

- Ashjian, C. J., S. L. Smith, C. N. Flagg, A. J. Mariano, W. J. Behrens, and P. V. Z. Lane (1994), The influence of a Gulf Stream meander on the distribution of zooplankton biomass in the Slope Water, the Gulf Stream, and the Sargasso Sea, described using a shipboard acoustic Doppler current profiler, *Deep Sea Res., Part I*, *41*, 23–50.
- Ashjian, C. J., S. L. Smith, C. N. Flagg, and N. Idrisi (2002), Distribution, annual cycle, and vertical migration of acoustically derived biomass in the Arabian Sea during 1994–1995, *Deep Sea Res., Part II*, *49*, 2377–2402.
- Batchelder, H. P., J. R. Vankeuren, R. Vaillancourt, and E. Swift (1995), Spatial and temporal distributions of acoustically estimated zooplankton biomass near the Marine Light-Mixed Layers station (59° 30'N, 21° 00'W) in the North Atlantic in May 1991, *J. Geophys. Res.*, *100*, 6549–6563.
- Behagle, N., L. du Buisson, E. Josse, A. Lebourges-Dhaussy, G. Roudaut, and F. Menard (2014), Mesoscale features and micronekton in the Mozambique Channel: An acoustic approach, *Deep Sea Res., Part II*, *100*, 164–173.
- Benitez-Nelson, C. R., and D. J. McGillicuddy (2008), Mesoscale physical-biological-biogeochemical linkages in the open ocean: An introduction to the results of the E-Flux and EDDIES programs—Preface, *Deep Sea Res., Part II*, *55*, 1133–1138.
- Burd, B. J., and R. E. Thomson (2012), Estimating zooplankton biomass distribution in the water column near the Endeavour Segment of Juan de Fuca Ridge using acoustic backscatter and concurrently towed nets, *Oceanography*, *25*, 269–276.
- Ceccarelli, D. M., et al. (2013), The coral sea: Physical environment, ecosystem status and biodiversity assets, in *Advances in Marine Biology*, vol. 66, edited by M. Lesser, pp. 213–290, Academic Press, Waltham, Mass.
- Chelton, D. B., P. Gaube, M. G. Schlax, J. J. Early, and R. M. Samelson (2011), The influence of nonlinear mesoscale eddies on near-surface oceanic chlorophyll, *Science*, *334*, 328–332.
- Cotté, C., F. d'Ovidio, A. Chaigneau, M. Lévy, I. Taupier-Letage, and C. Guinet (2011), Scale-dependent interactions of resident Mediterranean whales with marine dynamic, *Limnol. Oceanogr. Methods*, *56*, 219–232.
- Couvelard, X., P. Marchesiello, L. Gourdeau, and J. Lefevre (2008), Barotropic zonal jets induced by islands in the southwest Pacific, *J. Phys. Oceanogr.*, *38*, 2185–2204.
- David, P. M., O. Guerin-Ancey, and J. P. Van Cuyck (1999), Acoustic discrimination of two zooplankton species (mysid) at 38 and 120 kHz, *Deep Sea Res., Part I*, *46*(2), 319–333.
- Davis, C. S., and P. H. Wiebe (1985), Macrozooplankton biomass in a warm-core Gulf Stream Ring' time series changes in size structure, taxonomic composition, and vertical distribution, *J. Geophys. Res.*, *90*, 8871–8884.
- Deines, K. L. (1999), Backscatter estimation using Broadband Acoustic Doppler Current Profiles, in *Sixth Working Conference on Current Measurement*, vol. 1, edited by S. P. Anderson, et al., pp. 249–253, EEE, San Diego, Calif.
- D'Ovidio, F., V. Fernandez, E. Hernandez-Garcia, and C. Lopez (2004), Mixing structures in the Mediterranean Sea from finite-size Lyapunov exponents, *Geophys. Res. Lett.*, *31*, L17203, doi:10.1029/2004GL020328.
- D'Ovidio, F., E. Shuckburgh, and B. Legras (2009), Local mixing events in the upper troposphere and lower stratosphere. Part I: Detection with the Lyapunov Diffusivity, *J. Atmos. Sci.*, *66*, 3678.
- D'Ovidio, F., S. De Monte, A. Della Penna, C. Cotté, and C. Guinet (2013), Ecological implications of eddy retention in the open ocean: A Lagrangian approach, *J. Phys. A Math. Theor.*, *46*, doi:10.1088/1751-8113/46/25/254023.
- Espinasse, B., M. Zhou, Y. W. Zhu, E. L. Hazen, A. S. Friedlaender, D. P. Nowacek, D. Z. Chu, and F. Carloti (2012), Austral fall-winter transition of mesozooplankton assemblages and krill aggregations in an embayment west of the Antarctic Peninsula, *Mar. Ecol. Prog. Ser.*, *452*, 63–80.
- Fleminger, A., and R. I. Clutter (1965), Avoidance of towed nets by zooplankton, *Limnol. Oceanogr.*, *10*, 96–104.
- Gorsky, G., M. D. Ohman, M. Picheral, S. Gasparini, L. Stemmann, J. B. Romagnan, A. Cawood, S. Pesant, C. Garcia-Comas and F. Prejger (2010), Digital zooplankton image analysis using the ZooScan integrated system, *J. Plankton Res.*, *32*, 285–303.
- Gostiaux, L., and H. van Haren (2010), Extracting meaningful information from uncalibrated backscattered echo intensity data, *J. Atmos. Oceanic Technol.*, *27*, 943–949.
- Gourdeau, L., W. S. Kessler, R. E. Davis, J. Sherman, C. Maes, and E. Kestenare (2008), Zonal jets entering the coral sea, *J. Phys. Oceanogr.*, *38*, 715–725.
- Griffiths, F. B., and S. B. Brandt (1983), Mesopelagic crustacea in and around a warm-core eddy in the Tasmanian Sea off Eastern Australia, *Aust. J. Mar. Freshwater Res.*, *34*, 609–623.
- Grosjean, P., M. Picheral, C. Warembourg, and G. Gorsky (2004), Enumeration, measurement, and identification of net zooplankton samples using the ZOOscan digital imaging system, *ICES J. Mar. Sci.*, *61*(4), 518–525.
- Harris, R. P., P. Wiebe, J. Lenz, H. R. Skjoldal, and M. Huntley (2000), *Zooplankton Methodology Manual*, Academic, London, U. K.
- Hays, G. C., C. A. Proctor, A. W. G. John, and A. J. Warner (1994), Interspecific differences in the diel vertical migration of marine copepods: The implications of size, color, and morphology, *Limnol. Oceanogr.*, *39*(7), 1621–1629.
- Hernandez-Leon, S., C. Almeida, M. Gomez, S. Torres, I. Montero, and A. Portillo Hahnfeld (2001), Zooplankton biomass and indices of feeding and metabolism in island-generated eddies around Gran Canaria, *J. Mar. Syst.*, *30*, 51–66.
- Heywood, K. J., S. Scrope-Howe, and E. D. Barton (1991), Estimation of zooplankton abundance from shipborne ADCP backscatter, *Deep Sea Res., Part A*, *38*, 667–691.
- Holliday, D. V., and R. E. Pieper (1995), Bioacoustical oceanography at high frequencies, *ICES J. Mar. Sci.*, *52*, 279–296.
- Hosie, G. W., and T. G. Cochran (1994), Mesoscale distribution patterns of macrozooplankton communities in Prydz Bay, Antarctica—January to February 1991, *Mar. Ecol. Prog. Ser.*, *106*, 21–39.
- Hunt, B. P. V., V. Allain, C. Menkes, A. Lorrain, B. Graham, M. Rodier, M. Pagano, and F. Carloti (2014), A coupled stable isotope-size spectrum approach to understanding pelagic food-web dynamics: a case study from the southwest sub-tropical Pacific, *Deep Sea Res. Part II*, *113*, 208–224.
- Jiang, S., T. D. Dickey, D. K. Steinberg, and L. P. Madin (2007), Temporal variability of zooplankton biomass from ADCP backscatter time series data at the Bermuda Testbed Mooring site, *Deep Sea Res., Part I*, *54*, 608–636.
- Labat, J.-P. H., S. Gasparini, L. Mousseau, L. Prieur, M. Boutoute, and P. Mayzaud (2009), Mesoscale distribution of zooplankton biomass in the northeast Atlantic Ocean determined with an optical plankton counter: Relationships with environmental structures, *Deep Sea Res., Part I*, *56*, 1742–1756, doi:10.1016/j.dsr.2009.05.013.
- Lavery, A. C., D. Z. Chu, and J. N. Moum (2010), Measurements of acoustic scattering from zooplankton and oceanic microstructure using a broadband echosounder, *ICES J. Mar. Sci.*, *67*(2), 379–394.
- Le Borgne, R., M. Rodier, A. LeBouteiller, and M. Kulbicki (1997), Plankton biomass and production in an open atoll lagoon: Uvea, New Caledonia, *J. Exp. Mar. Biol. Ecol.*, *212*, 187–210.
- Le Borgne, R., P. Douillet, R. Fichez, and J.-P. Torreton (2010), Hydrography and plankton temporal variabilities at different time scales in the southwest lagoon of New Caledonia: A review, *Mar. Pollut. Bull.*, *61*, 297–308.

- Le Borgne, R., V. Allain, R. J. Matear, S. P. Griffiths, A. D. McKinnon, A. J. Richardson, and J. W. Young (2011), Vulnerability of open ocean food webs in the tropical Pacific to climate change, in *Vulnerability of Fisheries and Aquaculture in the Tropical Pacific to Climate Change*, edited by J. Bell, J. E. Johnson, and A. J. Hobday, Secr. of the Pac. Community, Noumea.
- Lebourges-Dhaussy, A., J. Coetzee, L. Hutchings, G. Roudaut and C. Nieuwenhuys (2009), Zooplankton spatial distribution along the South African coast studied by multifrequency acoustics, and its relationships with environmental parameters and anchovy distribution, *ICES J. Mar. Sci.*, *66*, 1055–1062.
- Lebourges-Dhaussy, A., J. Huggett, S. Ockhuis, G. Roudaut, E. Josse, and H. Verheye (2014), Zooplankton size and distribution within meso-scale structures in the Mozambique Channel: A comparative approach using the TAPS acoustic profiler, a multiple net sampler and Zoo-Scan image analysis, *Deep Sea Res., Part II*, *100*, 136–152.
- Lévy, M. (2008), The modulation of biological production by oceanic mesoscale turbulence, *Lect. Notes Phys.*, *744*, 219–261, doi:10.1007/978-3-540-75215-8_9.
- Longhurst, A. R. (2007), *Ecological Geography of the Sea*, 2nd ed., Elsevier Acad., Waltham, Mass.
- Luo, J. G., P. B. Ortner, D. Forcucci, and S. R. Cummings (2000), Diel vertical migration of zooplankton and mesopelagic fish in the Arabian Sea, *Deep Sea Res., Part II*, *47*, 1451–1473.
- MacLennan, D. N., P. G. Fernandes, and J. Dalen (2002), A consistent approach to definitions and symbols in fisheries acoustics, *ICES J. Mar. Sci.*, *59*, 365–369, doi:10.1006/jmsc.2001.1158.
- Marchesiello, P., J. Lefevre, A. Vega, X. Couvelard, and C. Menkes (2010), Coastal upwelling, circulation and heat balance around New Caledonia's barrier reef, *Mar. Pollut. Bull.*, *61*, 432–448.
- McGillicuddy, D. J., A. R. Robinson, D. A. Siegel, H. W. Jannasch, R. Johnson, T. Dickey, J. McNeil, A. F. Michaels, and A. H. Knap (1998), Influence of mesoscale eddies on new production in the Sargasso Sea, *Nature*, *394*, 263–266.
- McGillicuddy, D. J., et al. (2007), Eddy/wind interactions stimulate extraordinary mid-ocean plankton blooms, *Science*, *316*, 1021–1026.
- McKinnon, A. D., S. Duggan, and G. De'ath (2005), Mesozooplankton dynamics in nearshore waters of the Great Barrier Reef, *Estuarine Coastal Shelf Sci.*, *63*(4), 497–511.
- McNeil, J. D., H. W. Jannasch, T. Dickey, D. McGillicuddy, M. Brzezinski, and C. M. Sakamoto (1999), New chemical, bio-optical and physical observations of upper ocean response to the passage of a mesoscale eddy off Bermuda, *J. Geophys. Res.*, *104*, 15,537–15,548.
- Menkes, C. E., et al. (2014), Seasonal oceanography from physics to micronekton in the south-west Pacific, *Deep Sea Res., Part II*, *113*, 125–144, doi:10.1016/j.dsr2.2014.10.026.
- Moliner, J. C., F. Ibanez, S. Souissi, E. Bosc, and P. Nival (2008), Surface patterns of zooplankton spatial variability detected by high frequency sampling in the NW Mediterranean. Role of density fronts, *J. Mar. Syst.*, *69*(3–4), 271–282.
- Mutlu, E. (2003), Acoustical identification of the concentration layer of a copepod species, *Calanus euxinus*, *Mar. Biol.*, *142* (3), 517–523.
- Nowaczyk, A., F. Carlotti, D. Thibault-Botha, and M. Pagano (2011), Distribution of epipelagic metazooplankton across the Mediterranean Sea during the summer BOUM cruise, *Biogeosciences*, *8*, 2159–2177.
- Paffenhöfer, G. A., and M. G. Mazzocchi (2003), Vertical distribution of subtropical epipelagic copepods, *J. Plankton Res.*, *25*(9), 1139–1156.
- Pearre, S. (2003), Eat and run? The hunger/satiation hypothesis in vertical migration: History, evidence and consequences, *Biol. Rev.*, *78*(1), 1–79.
- Picheral, M. (2011), *ZOOPROCESS Manual*, 16 pp., Lab. d'Océanologie de Villefranche sur mer, France.
- Pieper, R. E., and D. V. Holliday (1984), Acoustic measurements of zooplankton distributions in the sea, *J. Cons. Cons. Int. Explor. Mer*, *41*, 226–238.
- Pieper, R. E., D. E. McGehee, C. F. Greenlaw and D. V. Holliday (2001), Acoustically measured seasonal patterns of Zooplankton in the Arabian Sea, *Deep Sea Res., Part II*, *48*, 1325–1343, doi:10.1016/S0967-0645(00)00141-7.
- Qiu, B., R. B. Scott, and S. M. Chen (2008), Length scales of eddy generation and nonlinear evolution of the seasonally modulated South Pacific Subtropical Countercurrent, *J. Phys. Oceanogr.*, *38*, 1515–1528.
- Radenac, M. H., P. E. Plimpton, A. Lebourges-Dhaussy, L. Commien, and M. J. McPhaden (2010), Impact of environmental forcing on the acoustic backscattering strength in the equatorial Pacific: Diurnal, lunar, intraseasonal, and interannual variability, *Deep Sea Res., Part II*, *57*, 1314–1328.
- Razouls, C., F. De Bovée, J. Kouwenberg, and N. Desreumaux (2005–2014), Diversité et répartition géographique chez les Copépodes planctoniques marins. [Available at <http://copepodes.obs-banyuls.fr>, <http://copepodes.obs-banyuls.fr>].
- Roman, M. R., H. G. Dam, R. Le Borgne, and X. Zhang (2002), Latitudinal comparisons of equatorial Pacific zooplankton, *Deep Sea Res., Part II*, *49*, 2695–2711.
- Shannon, C. E., and G. Weaver (1949), *The Mathematical Theory of Communication*, Univ. of Ill. Press, Urbana.
- Smeti, H. E., S. Jiang, M. H. Conte, and T. D. Dikey (2010), Mesoscale eddies enhance macrozooplankton abundance and carbon export to the deep ocean in the northwestern Sargasso Sea, *Eos Trans. AGU*, *91*(26), Ocean Sci. Meet. Suppl., Abstract B025G-16.
- Smith, S. L., and P. V. Z. Lane (1991), The jet off Point Arena, California: Its role in aspects of secondary production in the copepod *Eucalanus californicus* Johnson, *J. Geophys. Res.*, *96*, 14,849–14,858.
- Stanton, T. K., P. H. Wiebe, D. Z. Chu, M. C. Benfield, L. Scanlon, L. Martin, and R. L. Eastwood (1994), On acoustic estimates of zooplankton biomass, *ICES J. Mar. Sci.*, *51*, 505–512.
- Suthers, I. M., et al. (2011), The strengthening East Australian Current, its eddies and biological effects—An introduction and overview, *Deep Sea Res., Part II*, *58*, 538–546.
- Sutor, M. M., T. J. Cowles, W. T. Peterson, and S. D. Pierce (2005), Acoustic observations of finescale zooplankton distributions in the Oregon upwelling region, *Deep Sea Res., Part II*, *52*, 109–121.
- Tranter, D. J., G. S. Leech, and D. Airey (1983), Edge enrichment in an ocean eddy, *Aust. J. Mar. Freshwater Res.*, *34*, 665–680.
- Trégouboff, G., and M. Rose (1957), Manuel de planctologie méditerranéenne, in *Scientifique*, 587 pp., Centre national de la recherche scientifique, Paris.
- Wiebe, P. H., S. Boyd, and J. L. Cox (1975), Relationships between zooplankton displacement volume, wet weight, dry weight, and carbon, *Fish. Bull.*, *73*, 777–786.
- Wiebe, P. H., E. M. Hulbert, E. J. Carpenter, A. E. Jahn, G. P. Knapp, S. H. Boyd, P. B. Ortner, and J. L. Cox (1976), Gulf Stream cold core rings: Large-scale interaction sites for open ocean plankton communities, *Deep Sea Res. Oceanogr. Abstr.*, *23*, 695–710.
- Wiebe, P. H., C. H. Greene, T. K. Stanton, and J. Burczynski (1990), Sound scattering by live zooplankton and micronekton: Empirical studies with a dual-beam acoustical system, *J. Acoust. Soc. Am.*, *88*, 2346–2360.
- Wiebe, P. H., G. L. Lawson, A. C. Lavery, N. J. Copley, E. Horgan, and A. Bradley (2013), Improved agreement of net and acoustical methods for surveying euphausiids by mitigating avoidance using a net-based LED strobe light system, *ICES J. Mar. Sci.*, *70*, 650–664.

- Yebra, L., R. P. Harris, E. J. H. Head, I. Yashayaev, L. R. Harris, and A. G. Hirst (2009), Mesoscale physical variability affects zooplankton production in the Labrador Sea, *Deep Sea Res., Part I*, 56, 703–715.
- Young, J. W., A. J. Hobday, R. A. Campbell, R. J. Kloser, P. I. Bonham, L. A. Clementson, and M. J. Lansdell (2011), The biological oceanography of the East Australian Current and surrounding waters in relation to tuna and billfish catches off eastern Australia, *Deep Sea Res., Part II*, 58, 720–733.
- Zhou, M., W. Nordhausen, and M. Huntley (1994), ADCP measurements of the distribution and abundance of euphausiids near the Antarctic Peninsula in winter, *Deep Sea Res., Part I*, 41, 1425–1445.